AD_____

Award Number: W81XWH-09-1-0025

TITLE: Early Assessment of Breast Cancer Therapy Response Using Photoacoustic Molecular Imaging

PRINCIPAL INVESTIGATOR: Adam de la Zerda, BSc, MSc

CONTRACTING ORGANIZATION: LELAND STANFORD JUNIOR UNIVERSITY
THE STANFORD, CA 94305-5014

REPORT DATE: January 2010

TYPE OF REPORT: Annual Summary

PREPARED FOR: U.S. Army Medical Research and Materiel Command
Fort Detrick, Maryland 21702-5012

REPORT DOCUMENTATION PAGE

Form Approved
OMB No. 0704-0188

1. REPORT DATE	2. REPORT TYPE	3. DATES COVERED *(From - To)*
01-01-2010	Annual Summary	1 Jan 2009 – 31 Dec 2009

4. TITLE AND SUBTITLE
Early Assessment of Breast Cancer Therapy Response Using Photoacoustic Molecular Imaging

5a. CONTRACT NUMBER

5b. GRANT NUMBER
W81XWH-09-1-0025

5c. PROGRAM ELEMENT NUMBER

6. AUTHOR(S)
Adam de la Zerda

5d. PROJECT NUMBER

5e. TASK NUMBER

5f. WORK UNIT NUMBER

7. PERFORMING ORGANIZATION NAME(S) AND ADDRESS(ES)

LELAND STANFORD JUNIOR
UNIVERSITY, THE
STANFORD, CA 94305-5014

8. PERFORMING ORGANIZATION REPORT NUMBER

9. SPONSORING / MONITORING AGENCY NAME(S) AND ADDRESS(ES)
U.S. Army Medical Research and Materiel Command
Fort Detrick, Maryland 21702-5012

10. SPONSOR/MONITOR'S ACRONYM(S)

11. SPONSOR/MONITOR'S REPORT NUMBER(S)

12. DISTRIBUTION / AVAILABILITY STATEMENT
Approved for public release

13. SUPPLEMENTARY NOTES

14. ABSTRACT
The purpose of this grant is to build cancer-specific contrast agents for photoacoustic imaging, using which one could estimate the change in molecular expression of various breast-cancer-specific proteins undergoing chemotherapy treatment. We've made significant progress towards obtaining this goal: 1) we created the first-ever photoacoustic imaging agent (which is based on carbon nanotube nanoparticle) and showed it can specifically target tumors in tumor-bearing mice (paper published in Nature Nanotechnology); 2) We created 2 additional molecular imaging agents for photoacoustic imaging which exhibit 300-times higher sensitivity and for the first allow imaging photoacoustic molecular probes at sub-nanomolar concentrations (paper submitted to Nano Letters). We've shown that such sensitivity improvement results in the ability to image smaller tumors. Beyond higher sensitivity, the 3 imaging agents developed in this grant thus far have different optical spectra. We used this fact and have shown the ability to simultaneously image these agents (multiplexing). This ability is particularly powerful and important for this grant as we plan to progress to characterizing the response to chemotherapy of *multiple* cancer-specific proteins in the same tumor simultaneously.

15. SUBJECT TERMS
Photoacoustic Imaging, Molecular Imaging

16. SECURITY CLASSIFICATION OF:			17. LIMITATION OF ABSTRACT	18. NUMBER OF PAGES	19a. NAME OF RESPONSIBLE PERSON
a. REPORT	b. ABSTRACT	c. THIS PAGE			USAMRMC
U	U	U	UU	31	19b. TELEPHONE NUMBER *(include area code)*

Table of Contents

1. INTRODUCTION

The purpose of this grant is to build cancer-specific contrast agents for photoacoustic imaging, using which one could estimate the change in molecular expression of various breast-cancer-specific proteins undergoing chemotherapy treatment. We've made significant progress towards obtaining this goal: 1) we created the first-ever photoacoustic imaging agent (which is based on carbon nanotube nanoparticle) and showed it can specifically target tumors in tumor-bearing mice (paper published in Nature Nanotechnology); 2) We created 2 additional molecular imaging agents for photoacoustic imaging which exhibit 300-times higher sensitivity and for the first allow imaging photoacoustic molecular probes at sub-nanomolar concentrations (paper submitted to Nano Letters). We've shown that such sensitivity improvement results in the ability to image smaller tumors. Beyond higher sensitivity, the 3 imaging agents developed in this grant thus far have different optical spectra. We used this fact and have shown the ability to simultaneously image these agents (multiplexing). This ability is particularly powerful and important for this grant as we plan to progress to characterizing the response to chemotherapy of *multiple* cancer-specific proteins in the same tumor simultaneously.

2. BODY

2.1 Creation of 2 new Photoacoustic imaging agents

We have recently reported on the conjugation of cyclic Arg-Gly-Asp (RGD) peptides to pegylated SWNTs[1] and their use as photoacoustic imaging agents[2]. In order to enhance the photoacoustic signal of the SWNTs, we attached Indocyanine Green (ICG) and QSY-21 dyes to the surface of the SWNTs through pi-pi stacking interactions[3] (see Methods section for more details). The ultra-high surface area of SWNTs allows highly efficient loading of aromatic molecules such as ICG and QSY-21 on the nanotube surface. This created two new kinds of photoacoustic agents; SWNT-ICG and SWNT-QSY (**Fig. 1a)**. The particles were targeted using the RGD-peptide to $\alpha_v\beta_3$ integrins, which are over-expressed in tumor vasculature, while control untargeted particles were synthesized using a non-targeted peptide, RAD.

The optical absorbance spectra of the two new particles suggest that 710 nm and 780 nm are the preferable wavelengths for scanning SWNT-QSY and SWNT-ICG respectively (**Fig. 1b**). At their respective absorbance peaks, the SWNT-QSY and SWNT-ICG particles exhibit a 17 and 20-fold higher absorbance respectively as compared with plain SWNTs. Since blood absorption is significantly reduced at 780 nm compared to 710 nm, SWNT-ICG was the particle of choice for the small animal experiments for this study. Importantly, the attachment of RGD or RAD peptides to SWNT-ICG had little effect on the particles' absorbance. We constructed a non-absorbing and non-scattering agarose phantom with inclusions of SWNT-ICG-RGD at increasing concentrations from 0.5 nM to 121.5 nM in multiples of 3 (n = 3 samples of each concentration). The photoacoustic signal produced by the SWNT-ICG-RGD particles correlated well with the nanoparticle concentration (R^2=0.983) (**Fig. 1c**).

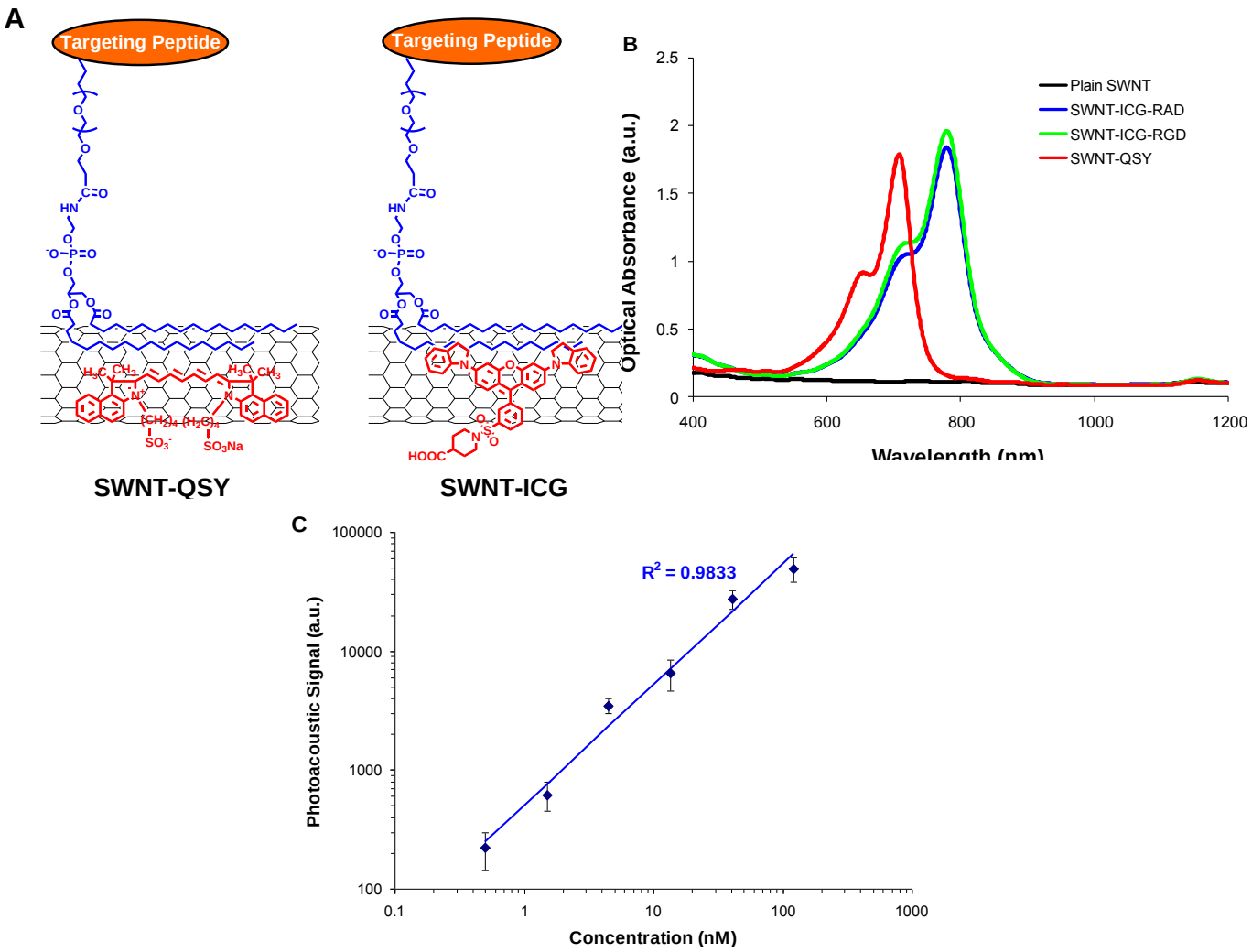

Figure 1. Characterization of the dye-enhanced SWNT. a, Illustration of SWNT-ICG and SWNT-QSY. ICG and QSY-21 (red molecules) are attached to the SWNT surface through non-covalent pi-pi stacking bonds. Polyethylene glycol-5000 (blue molecules) is conjugated to a targeting peptide in one end and to the SWNT surface on the other end through phospholipids. **b,** Optical spectra of plain SWNT (green), SWNT-ICG-RGD (red), SWNT-ICG-RAD (blue) and SWNT-QSY-RGD (black). The similarity of SWNT-ICG-RAD and SWNT-ICG-RGD spectra suggests that the peptide conjugation does not notably perturb the photoacoustic signal. **c,** The photoacoustic signal produced by SWNT-ICG was observed to be linearly dependent on the concentration (R^2 = 0.9833).

2.2 Sensitivity of the imaging agents in living mice

We then tested the particle's sensitivity in living subjects by subcutaneously injecting the lower back of mice (n = 3) with 30 μl of SWNT-ICG-RAD mixed with matrigel at increasing concentrations of 820 pM to 200 nM in multiples of 3. Matrigel alone produced no significant photoacoustic signal (data not shown). Upon injection, the matrigel solidified, fixing the SWNT-ICG-RAD in place and three-dimensional (3D) ultrasound and photoacoustic images of the inclusions were acquired (**Fig. 2a**). While the ultrasound images visualized the

mouse anatomy (e.g., skin and inclusion edges), the photoacoustic images revealed the SWNT-ICG-RAD contrast in the mouse. The photoacoustic signal from each inclusion was quantified using a three dimensional region of interest (ROI) drawn over the inclusion. We observed a linear correlation (R^2 = 0.97) between the SWNT-ICG-RAD concentration and the corresponding photoacoustic signal (**Fig. 2b**). Tissue background signal was calculated as the average photoacoustic signal in areas where no contrast agent was injected. Extrapolation of the signal-concentration graph reveals that 170 pM of SWNT-ICG-RAD gives the equivalent photoacoustic signal as the tissue background (i.e., signal to background ratio = 1). This value represents over 300-times improvement in sensitivity compared to plain SWNTs.

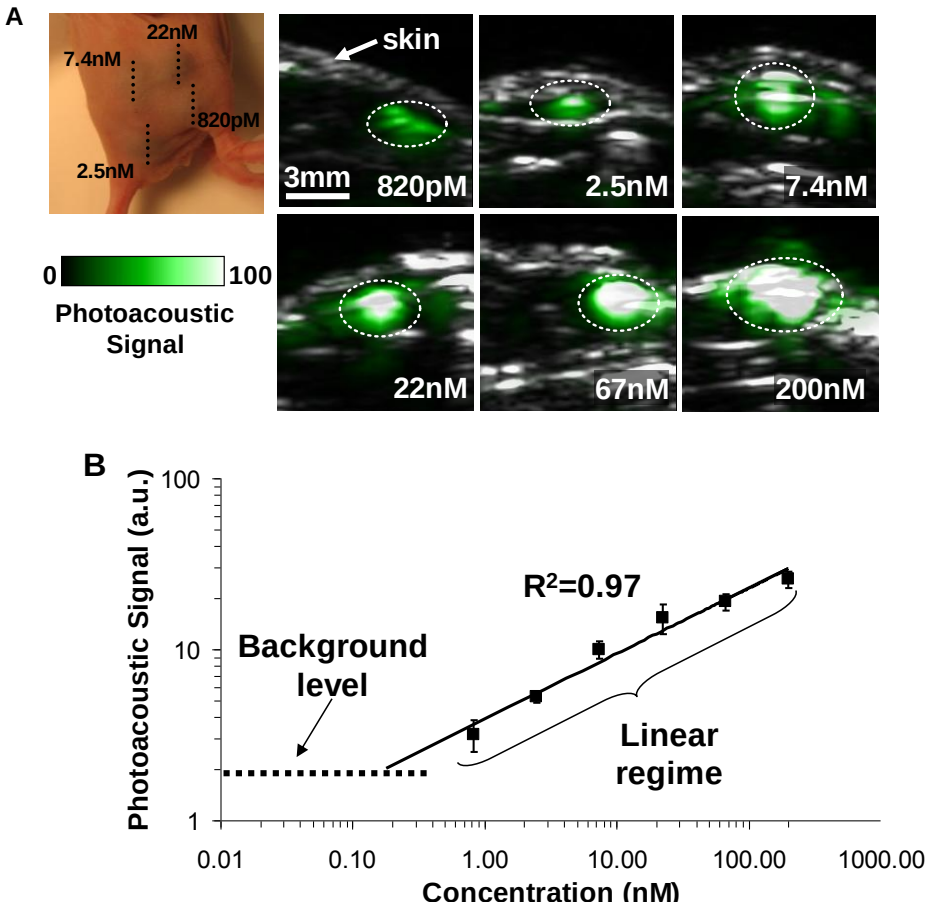

Figure 2. Photoacoustic detection of SWNT-ICG in living mice. a, Mice were injected subcutaneously with SWNT-ICG at concentrations of 0.82-200 nM. The images represent ultrasound (gray) and photoacoustic (green) vertical slices through the subcutaneous injections (dotted black line). The skin is visualized in the ultrasound images, while the photoacoustic images show the SWNT-ICG distribution. The white dotted lines on the images illustrate the approximate edges of each inclusion. **b,** The photoacoustic signal from each inclusion was calculated using 3D regions of interest and the „background' represents the endogenous signal measured from tissues. The error bars represent standard error (n = 3 mice). Linear regression (R^2 = 0.97) of the photoacoustic signal curve estimates that a concentration of 170 pM of SWNT-ICG will give the equivalent background signal of tissues.

2.3 Targeting of the imaging agents to tumors

Finally, we tested the nanoparticles targeting ability in living mice. Mice bearing tumor xenografts (150 mm^3 in size) were injected through the tail vein (IV) with 200 µl of either targeted SWNT-ICG-RGD or untargeted SWNT-ICG-RAD particles (n = 4 mice per group) at a concentration of 1.2 µM. We acquired 3D photoacoustic and ultrasound images of the entire tumor area before and up to 4 hours after the injection. Mice injected with the targeted SWNT-ICG-RGD particles show significantly higher photoacoustic signal in the tumor compared with the control group (**Fig. 3a**). The ultrasound images were used for visualizing the boundaries of the tumor as well as to validate that no significant movement (beyond 100 µm) had occurred throughout the scan. While the pre-injection photoacoustic signal is primarily due to the tumor's blood content, post-injection photoacoustic signal consists of both blood and SWNT-ICG. To subtract out the blood signal from the images, a subtraction image calculated as the 2 hour post-injection minus the pre-injection image was calculated. Measurement of the photoacoustic signal from a 3D ROI around the tumor (**Fig. 3b)** showed that the photoacoustic signal in the tumor was significantly higher in mice injected with SWNT-ICG-RGD as compared with the control particles SWNT-ICG-RAD ($p < 0.001$). For example, at 2 hours post-injection, mice injected with SWNT-ICG-RGD showed over 100% higher photoacoustic signal in the tumor than mice injected with the control SWNT-ICG-RAD.

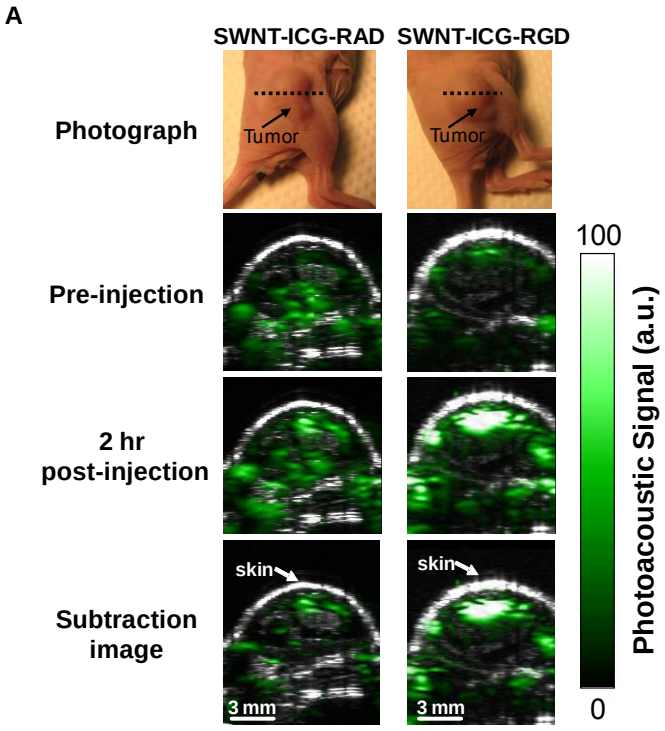

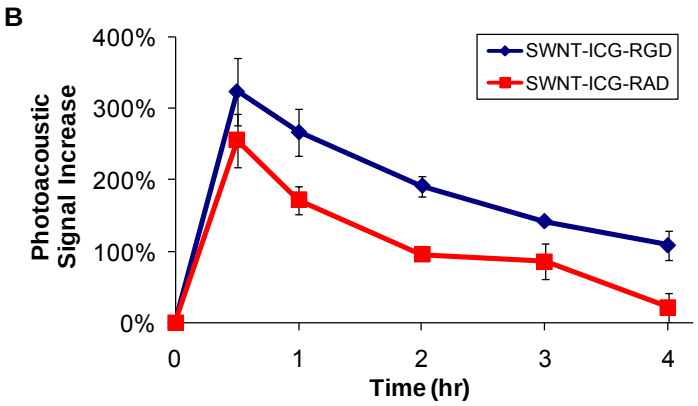

Figure 3. SWNT-ICG-RGD tumor targeting in living mice. a, Ultrasound (gray) and photoacoustic (green) images of one vertical slice through the tumor (dotted black line). The ultrasound images show the skin and the tumor boundaries. Subtraction photoacoustic images were calculated as 2 hr post-injection minus pre-injection images. As can be seen in the subtraction images, SWNT-ICG-RGD accumulates in higher amount in the tumor as compared to the control SWNT-ICG-RAD. **b,** Mice injected with SWNT-ICG-RGD showed significantly higher photoacoustic signal than mice injected with the untargeted control SWNT-ICG-RAD ($p < 0.001$). The error bars represent standard error (n = 4 mice)

2.4 Imaging the two contrast agents simultaneously (Multiplexing)

Finally, we show that the two kinds of photoacoustic imaging agents we synthesized, SWNT-ICG and SWNT-QSY can be imaged simultaneously due to their unique, though overlapping, absorbance spectra (**Fig. 1b**). We created an agarose gel phantom containing increasing concentrations of SWNT-ICG and decreasing concentrations of SWNT-QSY (starting from 100nM:0nM up to 0nM:100nM respectively). Photoacoustic images of the phantom were taken at wavelengths of 700, 730, 760, 780, and 800 nm and a spectral un-mixing algorithm was then used to separate each particle's signal to an individual image (**Fig. 4**).

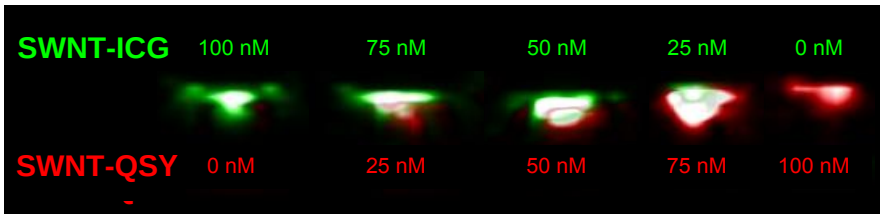

Figure 5. Multiplexing of SWNT-ICG with SWNT-QSY particles in a phantom. A phantom with various concentrations of SWNT-ICG and SWNT-QSY was scanned under the photoacoustic instrument at wavelengths of 700, 730, 760, 780, and 800 nm. A spectral un-mixing algorithm based on least-squares was used to separate the signals of SWNT-ICG particles (green) from SWNT-QSY particles (red). Notice that no SWNT-QSY signal is seen in the well with pure SWNT-ICG and vice versa, despite the fact that the two particles have overlapping spectra.

KEY RESEARCH ACCOMPLISHMENTS

- Developed two more photoacoustic imaging agents
- Characterized the particles and optimized them for tumor targeting upon intra-venous administration to tumor-bearing mice
- Optimized the imaging system to allow imaging the two imaging agents simultaneously

REPORTABLE OUTCOMES

- **Paper submitted: Adam de la Zerda**[*], Zhuang Liu[*], Sunil Bodapati, Cristina Zavaleta, Omer Oralkan, Hongjie Dai, Butrus T. Khuri-Yakub, Sanjiv S. Gambhir, "Enhanced Carbon Nanotubes for Photoacoustic Molecular Imaging in Living Mice", submitted to *Nature Photonics* (2009). ([*] equal contribution)
- **Paper published: Adam de la Zerda**, Cristina Zavaleta, Shay Keren, Srikant Vaithilingam, Sunil Bodapati, Zhuang Liu, Jelena Levi, Te-Jen Ma, Omer Oralkan, Zhen Cheng**,** Xiaoyuan Chen, Hongjie Dai, Butrus T. Khuri-Yakub, Sanjiv S. Gambhir, "Photoacoustic Molecular Imaging in Living Mice Utilizing Targeted Carbon Nanotubes", *Nature Nanotechnology*, 3, 557-62 (2008).
  Paper featured in: *Washington Post, US News, Forbes, USA Today, KCBS Radio, KGO Radio, KQED Radio, NCI Alliance for Nanotechnology in Cancer Newspaper, WECT TV6, Yahoo! News, Imperial Valley News, Wave 3, WGEM News* and more.
- **Abstract presented: A. de la Zerda**, Z. Liu, S. Bodapati, R. Teed, C. Zavaleta, S. Vaithilingam, X. Chen, B. T. Khuri-Yakub, H. Dai, S. S. Gambhir, "Ultra High Sensitivity Targeted Photoacoustic Imaging Agents for Cancer Early Detection in Living Mice", *World Molecular Imaging Congress* (2009)
- **Abstract presented: A. de la Zerda**, Z. Liu, C. Zavaleta, S. Bodapati, R. Teed, S.Vaithilingam, T. Ma, O. Oralkan, X. Chen, B. T. Khuri-Yakub, H. Dai, S. S. Gambhir "Enhanced Sensitivity Carbon Nanotubes as Targeted Photoacoustic Molecular Imaging Agents", Proceedings of SPIE Photonics West, 7177-93:3 1-8 (2009).
  Abstract poster presentation was awarded the best poster presentation at the Photoacoustic session at the conference – the biggest photoacoustic conference.
- **Abstract presented: A. de la Zerda**, C. Zavaleta, S. Keren, S. Vaithilingam, S. Bodapati, R. Teed, Z. Liu, J. Levi, B. R. Smith, T. Ma, O. Oralkan, Z. Cheng, X. Chen, H. Dai, B. T. Khuri-Yakub, S. S. Gambhir, "Photoacoustic Molecular Imaging using Single Walled Carbon Nanotubes in Living Mice", Proceedings of SPIE Photonics West, 7177-78:5 1-12 (2009).

CONCLUSION

The main achievement over this past year was the development of 2 new photoacoustic imaging agents which allow reaching unprecedented sensitivities. This development will be the basis for measuring breast cancer response to chemotherapy and will allow investigating biomarkers which weren't been able to investigate before due to insufficient sensitivity of photoacoustic instruments.

REFERENCES

1. **Liu, Z. et al. In vivo biodistribution and highly efficient tumour targeting of carbon nanotubes in mice. Nat Nano 2, 47-52 (2007).**
2. **de la Zerda, A. et al. Carbon nanotubes as photoacoustic molecular imaging agents in living mice. Nat Nanotechnol 3, 557-62 (2008).**
3. **Liu, Z., Sun, X., Nakayama-Ratchford, N. & Dai, H. Supramolecular Chemistry on Water-Soluble Carbon Nanotubes for Drug Loading and Delivery. ACS Nano. 1, 50-56 (2007).**

APPENDICES

1. Paper published in Nature Nanotechnology:

Carbon nanotubes as photoacoustic molecular imaging agents in living mice

ADAM DE LA ZERDA[1,2], CRISTINA ZAVALETA[1], SHAY KEREN[1], SRIKANT VAITHILINGAM[3], SUNIL BODAPATI[1], ZHUANG LIU[3], JELENA LEVI[1], BRYAN R. SMITH[1], TE-JEN MA[2], OMER ORALKAN[2], ZHEN CHENG[1], XIAOYUAN CHEN[1], HONGJIE DAI[3], BUTRUS T. KHURI-YAKUB[2] AND SANJIV S. GAMBHIR[1,4]*

[1]Molecular Imaging Program at Stanford, Department of Radiology and Bio-X Program, Stanford University, Palo Alto, California 94305, USA
[2]Department of Electrical Engineering, Stanford University, Palo Alto, California 94305, USA
[3]Department of Chemistry, Stanford University, Palo Alto, California 94305, USA
[4]Department of Bioengineering, Stanford University, Palo Alto, California 94305, USA
*e-mail: sgambhir@stanford.edu

Published online: 17 August 2008; doi:10.1038/nnano.2008.231

Photoacoustic imaging of living subjects offers higher spatial resolution and allows deeper tissues to be imaged compared with most optical imaging techniques[1–7]. As many diseases do not exhibit a natural photoacoustic contrast, especially in their early stages, it is necessary to administer a photoacoustic contrast agent. A number of contrast agents for photoacoustic imaging have been suggested previously[8–15], but most were not shown to target a diseased site in living subjects. Here we show that single-walled carbon nanotubes conjugated with cyclic Arg-Gly-Asp (RGD) peptides can be used as a contrast agent for photoacoustic imaging of tumours. Intravenous administration of these targeted nanotubes to mice bearing tumours showed eight times greater photoacoustic signal in the tumour than mice injected with non-targeted nanotubes. These results were verified *ex vivo* using Raman microscopy. Photoacoustic imaging of targeted single-walled carbon nanotubes may contribute to non-invasive cancer imaging and monitoring of nanotherapeutics in living subjects[16].

Recently, we reported on the conjugation of cyclic RGD containing peptides to single-walled carbon nanotubes[17] (SWNT–RGD) that is stable in serum. The single-walled carbon nanotubes, which were 1–2 nm in diameter and 50–300 nm in length were coupled to the RGD peptides through polyethylene glycol-5000 grafted phospholipid (PL–PEG_{5000}). These SWNT–RGD conjugates bind with high affinity to $\alpha_v\beta_3$ integrin, which is over-expressed in tumour neovasculature, and to other integrins expressed by tumours but with lower affinity[18,19]. We also synthesized non-targeted single-walled carbon nanotubes (that is, plain single-walled carbon nanotubes) by conjugating them solely to PL–PEG_{5000} (Fig. 1a). Our photoacoustic instrument[20] used a single-element focused transducer to raster scan the object under study, which was illuminated through a fibre head (see Methods and Supplementary Information, Fig. S1). In a phantom study we measured the photoacoustic signal of plain single-walled carbon nanotubes and SWNT–RGD at wavelengths of 690–800 nm (Fig. 1b; shorter wavelengths are less desirable as the depth of penetration through the tissues is reduced[21]). These photoacoustic spectra suggest that 690 nm is the preferable wavelength, because the photoacoustic signal of the single-walled carbon nanotubes is highest at that wavelength. Furthermore, the ratio of single-walled carbon nanotubes to haemoglobin signal is higher at this wavelength when compared with other wavelengths. Importantly, the photoacoustic signal of single-walled carbon nanotubes was found to be unaffected by the RGD peptide conjugation. This finding was validated through measurements of the optical absorbance of the two single-walled carbon nanotubes conjugates (see Supplementary Information, Fig. S2). In a separate non-absorbing and non-scattering phantom study, we also validated that the photoacoustic signal produced by single-walled carbon nanotubes is in linear relationship with their concentration (Fig. 1c) with $R^2 = 0.9997$.

We then subcutaneously injected the lower back of a mouse with 30 µl of mixtures of single-walled carbon nanotubes and matrigel at concentrations between 50 and 600 nM ($n = 3$ for each concentration). Matrigel alone produced no photoacoustic signal (data not shown). Upon injection, the matrigel solidified, fixing the single-walled carbon nanotubes in place. Three-dimensional (3D) ultrasound and photoacoustic images of the inclusions were then acquired (Fig. 2a). The ultrasound images showed the mouse anatomy (for example, skin and inclusion edges), and the photoacoustic images revealed the single-walled carbon nanotubes contrast in the mouse. The photoacoustic signal from each inclusion was quantified using a 3D region of interest drawn over the inclusion. We observed a linear correlation ($R^2 = 0.9929$) between the single-walled carbon nanotubes concentration and the corresponding photoacoustic signal (Fig. 2b). Importantly, this linear relation can only be expected in special cases where the dye concentration does not perturb the tissue light distribution significantly. We concluded that the photoacoustic signal produced by tissues (background) was equivalent to the photoacoustic signal produced by 50 nM of single-walled carbon nanotubes (that is, a signal-to-background ratio of 1). This experimental result correlates well with the theoretical analysis (see Supplementary Information), which predicts a background signal equal to 7–70 nM of single-walled carbon nanotubes, depending on the location of the nanotubes in the body.

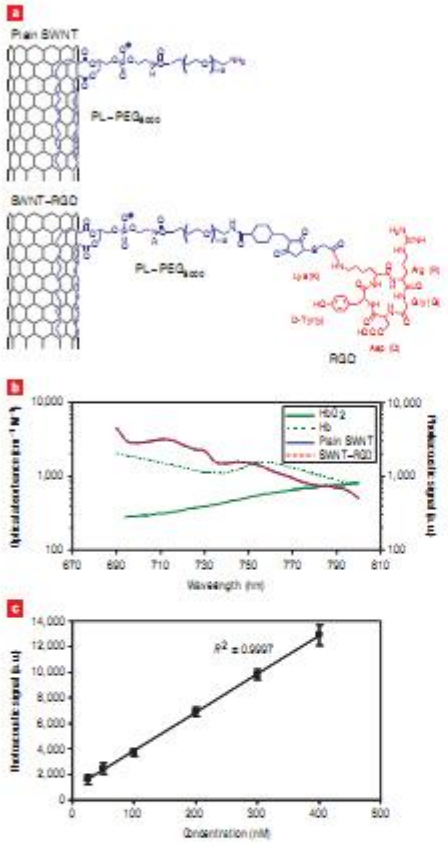

Figure 1 Characterization of the photoacoustic properties of single-walled carbon nanotubes. a, Illustration of plain single-walled carbon nanotubes (plain SWNT) and SWNT–RGD. The phospholipid binds to the sidewall of the single-walled carbon nanotubes connecting the PEG_{5000} to the nanotubes. The RGD allows the single-walled carbon nanotubes to bind to tumour integrins such as $\alpha_v\beta_3$. **b**, The photoacoustic spectra of plain single-walled carbon nanotubes and SWNT–RGD are overlaid on the known optical absorbance of HbO_2 and Hb. The spectral overlap between plain single-walled carbon nanotubes and SWNT–RGD suggests that the RGD conjugation does not perturb the photoacoustic signal. **c**, The photoacoustic signal produced by single-walled carbon nanotubes was observed to be linearly dependent on the concentration ($R^2 = 0.9997$).

We then injected two groups of mice bearing U87MG tumour xenografts (~100 mm^3) through the tail-vein (IV) with either 200 µl of plain single-walled carbon nanotubes ($n = 4$) or SWNT–RGD ($n = 4$) at a concentration of 1.2 µM.

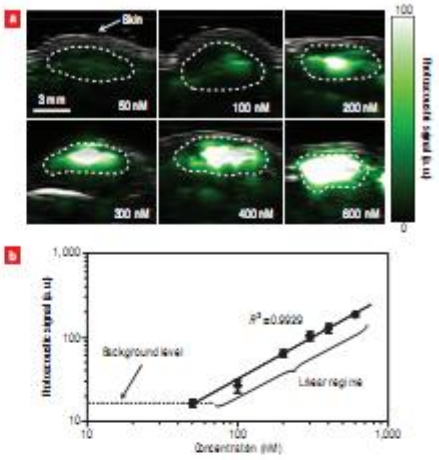

Figure 2 Photoacoustic detection of single-walled carbon nanotubes in living mice. a, Mice were injected subcutaneously with single-walled carbon nanotubes at concentrations of 50–600 nM. One vertical slice in the 3D photoacoustic image (green) was overlaid on the corresponding slice in the ultrasound image (grey). The skin is visible in the ultrasound images, and the photoacoustic images show the single-walled carbon nanotubes. The dotted lines on the images identify the edges of each inclusion. **b**, The photoacoustic signal from each inclusion was calculated. The background level represents the endogenous signal measured from tissues. The error bars represent standard error ($n = 3$). The linear regression is calculated on the five most concentrated inclusions ($R^2 = 0.9929$).

Three-dimensional ultrasound and photoacoustic images of the tumour and its surroundings were acquired before and up to 4 h after injection. We found that mice injected with SWNT–RGD showed a significant increase of photoacoustic signal in the tumour compared with control mice injected with plain single-walled carbon nanotubes (Fig. 3a). The images from the different time points were aligned with one another using simple vertical translations to account for small vertical movements in the transducer positioning. This alignment allowed quantification of the photoacoustic signal at all time points using a single region of interest. We then calculated a subtraction image between the photoacoustic image taken at 4 h post-injection and the photoacoustic image taken before injection. The subtraction image better visualizes the real distribution of the single-walled carbon nanotubes as it removes, to a large extent, the background signal. For example, in the mouse injected with plain single-walled carbon nanotubes (Fig. 3a), a high photoacoustic signal, likely produced by a large blood vessel, was seen in the pre-injection and post-injection images. However, the subtraction image showed a much lower signal from this area, reflecting the likely low concentration of plain single-walled carbon nanotubes there. We calculated the photoacoustic signal by drawing a 3D region of interest around the tumour (tumour boundaries were clearly visualized in the ultrasound images). The photoacoustic signal increase was quantified as a function of time

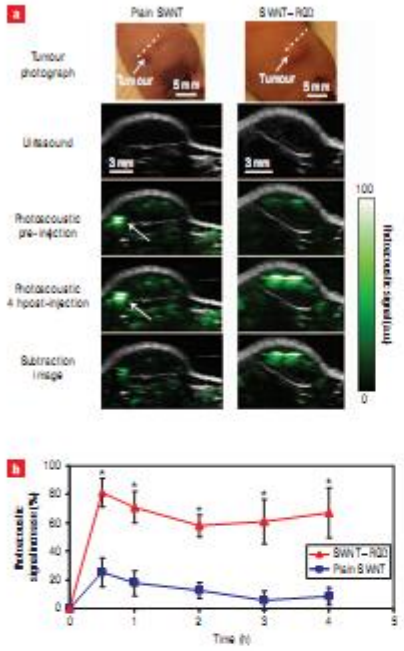

Figure 3 Single-walled carbon nanotube targets tumour in living mice. **a**, Ultrasound (grey) and photoacoustic (green) images of one vertical slice (white dotted line) through the tumour. The ultrasound images show the skin and tumour boundaries. Subtraction images were calculated as the 4 h post-injection image minus the pre-injection image. The high photoacoustic signal in the mouse injected with plain single-walled carbon nanotubes (indicated with a white arrow) is not seen in the subtraction image, suggesting that it is due to a large blood vessel and not single-walled carbon nanotubes. **b**, Mice injected with SWNT–RGD showed a significantly higher photoacoustic signal than mice injected with plain single-walled carbon nanotubes ($P < 0.001$). The error bars represent standard error ($n = 4$). *$P < 0.05$.

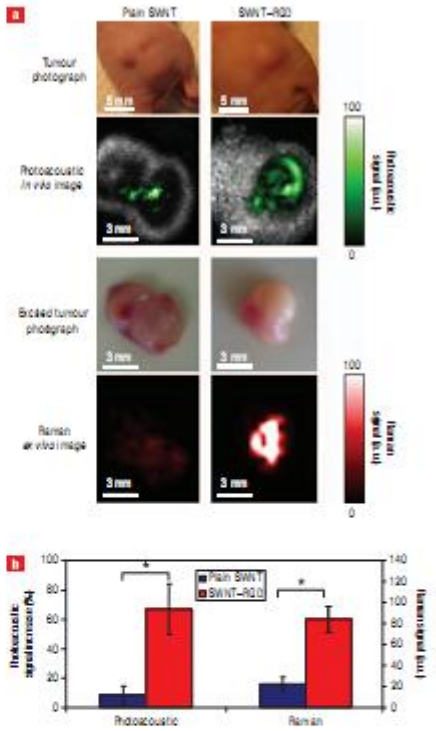

Figure 4 Validation of the *in vivo* photoacoustic images by Raman *ex vivo* microscopy. **a**, Photographs of the tumours in mice and the corresponding photoacoustic subtraction images (green) shown as horizontal slices through the tumours. After the photoacoustic scan, the tumours were excised and scanned using a Raman microscope (red). Mice injected with plain single-walled carbon nanotubes (left-hand column) showed both low photoacoustic and Raman signals compared with mice injected with SWNT–RGD (right-hand column). The tumours are in the same orientation in all images. **b**, Comparison between the photoacoustic signal of the tumours *in vivo* (left) and the Raman signal acquired from the excised tumours (right). *$P < 0.05$.

(Fig. 3b). Although SWNT–RGD led to a consistently higher photoacoustic signal, plain single-walled carbon nanotubes led only to a temporary increase in the photoacoustic signal of the tumour ($P < 0.001$ when comparing entire time-curves, and $P < 0.05$ when comparing the signals at each time point independently). The temporary photoacoustic signal observed for plain single-walled carbon nanotubes is likely caused by circulating nanotubes that are eventually cleared from the bloodstream. Conversely, SWNT–RGD bind to the tumour vasculature, creating a consistent photoacoustic signal from the tumour. On average, at 4 h post-injection, the SWNT–RGD resulted in ~8 times greater increase in photoacoustic signal compared with plain single-walled carbon nanotubes. The percentage injected dose per gram of tissue was calculated to be ~14 %ID g^{-1} (see Supplementary Information).

We further validated our photoacoustic results using a Raman microscope, as an independent method for detection of single-walled carbon nanotubes. At the conclusion of the photoacoustic study, 4 h post-injection, the mice were sacrificed; the tumours were surgically removed and scanned *ex vivo* under a Raman microscope. The two-dimensional Raman images of the excised tumours were found to match the photoacoustic images (Fig. 4a). The mean Raman signal from the tumours was calculated from the Raman images. Similarly to the photoacoustic results, the Raman signal from the tumours was ~4 times higher in mice injected with SWNT–RGD than in mice injected with plain single-walled carbon nanotubes (Fig. 4b).

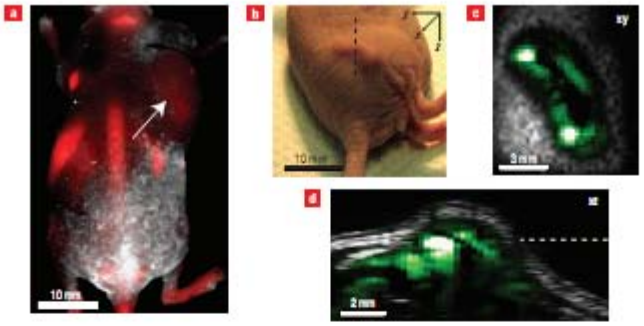

Figure 5 Comparison between photoacoustic imaging using single-walled carbon nanotubes and fluorescence imaging using quantum dots. a, Fluorescence image (red) of a mouse injected with QD–RGD. The white arrow indicates the tumour location. The other bright spots on the image represent the different organs in which QD–RGD non-specifically accumulated. b, Tumor photograph. c, Horizontal (xy plane) and d, vertical (xz plane) slices in the 3D photoacoustic image of a mouse injected with SWNT–RGD. The black dotted line shows the vertical slice orientation and the white dotted line shows the height of the horizontal slice in the vertical slice. The location of the single-walled carbon nanotubes in the tumour is visualized with high spatial resolution.

Unlike photoacoustic imaging, optical imaging suffers from relatively poor spatial resolution as well as exponentially degraded sensitivity as tissue depth increases[12]. We showed the superiority of our photoacoustic strategy by comparing it with fluorescence imaging of tumour-targeted quantum dots. The quantum dots were conjugated to RGD peptides[12] (QD–RGD) and imaged 6 h post-injection using a fluorescence imaging instrument (Fig. 5a). Although the quantum dot and single-walled carbon nanotube conjugates might have different biodistributions, the photoacoustic images of single-walled carbon nanotubes from the tumour illustrated the depth-information and the greater spatial resolution achieved by photoacoustic imaging compared with fluorescence imaging (Fig. 5b–d). The smeared signal from the tumour in the fluorescence image is due to light scattering. However, the photoacoustic images showed the 3D distribution of SWNT–RGD in the tumour with high spatial resolution. Similar results were also observed in a phantom study (see Supplementary Information, Fig. S4).

We have demonstrated that single-walled carbon nanotubes can be exploited as photoacoustic contrast agents to non-invasively image tumours. Intravenous injection of targeted single-walled carbon nanotubes in mice led to 8 times higher photoacoustic signal in the tumour compared with mice injected with non-targeted single-walled carbon nanotubes. Our photoacoustic images were verified using Raman microscopy on the surgically removed tumours. Furthermore, our results agreed with a previous study[17] where radiolabelled SWNT–RGD were monitored using small animal positron emission tomography (microPET). In that study SWNT–RGD were found to accumulate ~3–5 times more in tumours than plain single-walled carbon nanotubes. That study also showed that the SWNT–RGD did not accumulate in the tissue surrounding the tumour.

Most previous work on photoacoustic contrast agents *in vivo* is limited to non-targeted agents such as gold nanocages used for highlighting the blood vessels in a rat's brain[11]. A recent preliminary study[13] showed that an indocyanine green derivative (IRDye-800-c(KRGDf)) may be applicable for photoacoustic spectroscopic imaging of U87MG tumours; however, the study was carried out on a single mouse and statistical validation of the agent has yet to be shown. Various gold nanoparticles have been previously suggested, primarily for their high absorption characteristics and the ability to control their spectra, which allows multiplexing studies[9]. However, their main limitation is their relatively large size, which will lead to their rapid clearance by the reticuloendothelial system (RES) upon intravenous injection. It is possible that single-walled carbon nanotubes, due to their unique high aspect ratio (~1:100) and high surface area to volume ratio, are capable of minimizing RES uptake while having an increased affinity for molecular targets due to multivalency effects[17]. A concentration of 50 nM of single-walled carbon nanotubes was found to produce a photoacoustic signal equivalent to mouse tissues (background); however, the minimum detectable concentration of single-walled carbon nanotubes is likely to be less than 50 nM. This is because photoacoustic images were acquired before and after the administration of the contrast agent, thus making it possible to separate the contrast agent signal from the background signal. Further background reduction can be achieved by performing photoacoustic spectral imaging, improving hardware/reconstruction software, or by enhancing the single-walled carbon nanotubes' photoacoustic signal. With respect to acquisition time, our current instrument acquires a single photoacoustic image in ~20–30 minutes for a tumour ~100 mm^3 in size. However, by using lasers with higher repetition rates, scan duration can be greatly reduced.

We are currently investigating the potential of single-walled carbon nanotubes to extravasate out of the leaky vasculature of tumours. Single-walled carbon nanotube extravasation is of particular interest, because upon exiting the vasculature, the nanotubes would have access to many more molecular targets that exist only on the cancer cell's membranes. Future work should optimize the particles' extravasation as well as bring new technologies to help quantify the degree of nanotube extravasation. Moreover, future studies can monitor various nano-therapeutic applications such as drug-eluting single-walled

carbon nanotubes using photoacoustic imaging. Such nanotherapeutic and cancer imaging applications would gain further clinical interest as single-walled carbon nanotubes continue to show no toxic effects[24]. Although single-walled carbon nanotubes have the capability to efficiently bind to molecular targets, their high photoacoustic signal allows for high-resolution 3D photoacoustic images with substantial depth of penetration. None of the other molecular imaging modalities compares with the precise depth information and submillimetre resolution at nanomolar sensitivity that is achieved by photoacoustic imaging. We expect this work to stimulate further studies of biologically relevant problems using photoacoustic molecular imaging.

METHODS

SYNTHESIS OF SINGLE-WALLED CARBON NANOTUBE CONJUGATES

A complete description of the synthesis of SWNT–RGD and plain single-walled carbon nanotubes can be found elsewhere[17]. The single-walled carbon nanotubes used in this work were 50–300 nm in length and 1–2 nm in diameter. The molar concentrations[25] were based on an average molecular weight of 170 kDa per single-walled carbon nanotube (150 nm in length and 1.2 nm in diameter).

STATISTICAL METHODS

For the single-walled carbon nanotube tumour targeting experiments, we used a random-effects regression to test the hypothesis that mice injected with SWNT–RGD showed an increased photoacoustic signal over time in the tumour compared with the control group injected with plain single-walled carbon nanotubes. We also performed the one-tailed student's *t*-test at each time point independently to test whether the previous effect will be observed by sampling the photoacoustic signal at a single time point instead. For the cell uptake studies, we used the one-tailed student's *t*-test to test whether the group in which U87MG cells were exposed to SWNT–RGD had a statistically higher signal than each of the other groups independently.

PHOTOACOUSTIC INSTRUMENTATION

Our in-house photoacoustic system[26] is illustrated in the Supplementary Information, Fig. S1. A tuneable pulsed laser with a repetition rate of 10 Hz and a pulsewidth of 5 ns (Nd:YAG Sunlight-III-10 connected to Sunlite OPO Plus, Continuum) illuminated the object through a fibre-optic ring light (50-1353 Ringlight, Fiberoptic Systems). The average energy density of the laser at 690 nm wavelength was measured to be ~9 mJ cm^{-2} at the target site, which is below the ANSI limitation for laser skin exposure[26]. A 5 MHz focused transducer (25.5 mm focal length, 4 MHz bandwidth, F number of 2.0, depth of focus of 6.8 mm, lateral resolution of 600 μm and axial resolution of 380 μm; A3095-SU-F-24.5-MM-PTF, Panametrics) was used to acquire both pulse-echo and photoacoustic images. In addition, high-resolution ultrasound images were acquired using a 25 MHz focused transducer (27 mm focal length, 12 MHz bandwidth, F number of 4.2, depth of focus of 7.5 mm, lateral resolution of 250 μm and axial resolution of 124 μm; V324-SU-25.5-MM, Panametrics). A precision xyz-stage (US50, Aerotech) with minimum step size of 1 μm was used to move the transducer and the fibre ring along a planar 2D trajectory. At every position, the acquired signal was averaged over 16 laser pulses. The time of arrival and the intensity of the laser pulses were recorded using a silicon photodiode (DET10A, Thorlabs). This information was used to synchronize the acquisition and compensate for pulse-to-pulse variations in laser intensity. The analogue photoacoustic signals were amplified using a 40 dB preamplifier (5676/1.15VAC, Panametrics) and digitized using an oscilloscope (Infiniium 54825A, Agilent). The photoacoustic and ultrasound images were reconstructed as follows: the *a*-scan from each position of the transducer was bandpass-filtered with 100% fractional bandwidth, compensated for laser intensity variation and envelope detected. The *a*-scans were then combined to reconstruct a 3D intensity image of the target. No further post-processing was carried out on the images. The ultrasound images acquired using the 5 MHz and 25 MHz transducers were aligned together using small vertical translations so that the object's skin level matched in both images. The photoacoustic and high-frequency ultrasound images were analysed, co-registered, and displayed using AMIDE[27] software.

SINGLE-WALLED CARBON NANOTUBE TUMOUR TARGETING IN LIVING MICE

All animal experiments were performed in compliance with the Guidelines for the Care and Use of Research Animals established by the Stanford University Animal Studies Committee. Two groups of female nude mice ($n = 3$ in each group), 6–8 weeks old were inoculated subcutaneously at their lower right back with 10^7 U87MG cells (American Type Culture Collection, ATCC) suspended in 50 μl of saline (PBS, pH 7.4 1 × ,Invitrogen). The tumours were allowed to grow to a volume of ~100 mm^3. Before the injection of single-walled carbon nanotubes, photoacoustic and ultrasound images of the mice were taken. Photoacoustic excitation light was 690 nm. The single-walled carbon nanotubes were sonicated for 3 min under 1 W rms. (Sonifier 150, Branson) to separate single-walled carbon nanotubes that may have aggregated. The mice were then injected with 200 μl of 1.2 μM single-walled carbon nanotubes into the tail-vein. During the injection the positioning of the mice was not changed. After injection, photoacoustic and ultrasound images were acquired at 0.5, 1, 2, 3 and 4 h post injection. The scanning area varied between mice depending on the tumour orientation, but typically was ~80 mm^2, with a step size of 0.25 mm. At 4 h post-injection, the mice were killed and their tumours surgically removed for further *ex vivo* analysis. The ultrasound images from the different time points were aligned with one another by vertically translating the images (translation was typically less than 0.5 mm). The same alignment was then applied to the photoacoustic images. Using AMIDE software, a 3D region of interest was drawn over the tumour volume (which was clearly illustrated in the ultrasound images). The mean photoacoustic signal in the tumour region of interest was calculated for each photoacoustic image.

Received 10 December 2007; accepted 4 July 2008; published 17 August 2008.

References

1. Xu, M. H. & Wang, L. H. V. Photoacoustic imaging in biomedicine. *Rev. Sci. Instrum.* **77**, 041101 (2006).
2. Oh, J. T. *et al.* Three-dimensional imaging of skin melanoma *in vivo* by dual-wavelength photoacoustic microscopy. *J. Biomed. Opt.* **11**, 34032 (2006).
3. Zhang, H. F., Maslov, K., Stoica, G. & Wang, L. V. Imaging acute thermal burns by photoacoustic microscopy. *J. Biomed. Opt.* **11**, 054033 (2006).
4. Wang, X., Xie, X., Xu, G., Wang, L. V. & Stoica, G. Noninvasive imaging of hemoglobin concentration and oxygenation in the rat brain using high-resolution photoacoustic tomography. *J. Biomed. Opt.* **11**, 024015 (2006).
5. Zhang, H. F., Maslov, K., Stoica, G. & Wang, L. V. Functional photoacoustic microscopy for high-resolution and noninvasive *in vivo* imaging. *Nat. Biotechnol.* **24**, 848–851 (2006).
6. Manohar, S. *et al.* Initial results of *in vivo* non-invasive cancer imaging in the human breast using near-infrared photoacoustics. *Opt. Express* **15**, 12277–12285 (2007).
7. Emelianov, S. *et al.* Detection and noninvasive diagnostics of breast cancer with 2-colour laser optoacoustic imaging system. *Proc. SPIE* **6437**, 643703 (2007).
8. Eghtedari, M. *et al.* High sensitivity of *in vivo* detection of gold nanorods using a laser optoacoustic imaging system. *Nano Lett.* **7**, 1914–1918 (2007).
9. Li, P. C. *et al.* Photoacoustic imaging of multiple targets using gold nanorods. *IEEE Trans. Ultrason. Ferroelectr. Freq. Control* **54**, 1642–1647 (2007).
10. Kim, C. *et al.* Indocyanine-green-embedded PEBBLEs as a contrast agent for photoacoustic imaging. *J. Biomed. Opt.* **12**, 044020 (2007).
11. Yang, X., Skrabalak, S. E., Li, Z. Y., Xia, Y. & Wang, L. V. Photoacoustic tomography of a rat cerebral cortex *in vivo* with Au nanocages as an optical contrast agent. *Nano Lett.* **7**, 3798–3802 (2007).
12. Zharov, V. P. *et al.* Photoacoustic flow cytometry: principle and application for real-time detection of circulating single nanoparticles, pathogens and contrast dyes *in vivo*. *J. Biomed. Opt.* **12**, 051503 (2007).
13. Li, M.-L. *et al.* Simultaneous molecular and hypoxia imaging of brain tumors *in vivo* using spectroscopic photoacoustic tomography. *Proc. IEEE* **96**, 481–489 (2008).
14. Wu, C.-W. *et al.* *In vivo* photoacoustic imaging with multiple electromagnetic using bioconjugated gold nanorods. *Proc. SPIE* **6856**, 68560U (2008).
15. Kim, K. *et al.* *In vivo* imaging of inflammatory response by photoacoustics using all-trapped gold nanorods (GNR) as contrast agent. *Proc. SPIE* **6856**, 68560I (2008).
16. Branco, A., Konstadin, K. & Prato, M. Applications of carbon nanotubes in drug delivery. *Curr. Opin. Chem. Biol.* **9**, 674–679 (2005).
17. Liu, Z. *et al.* *In vivo* biodistribution and highly efficient tumour targeting of carbon nanotubes in mice. *Nature Nanotech.* **2**, 47–52 (2007).
18. Mikaelsen, O. J. Role of integrins in cancer survey of expression patterns. *Proc. Soc. Exp. Biol. Med.* **222**, 124–138 (1999).
19. Janssen, M. L. *et al.* Tumour targeting with radiolabelled alpha(v)beta(3) integrin binding peptides in a nude mouse model. *Cancer Res.* **62**, 6146–6151 (2002).
20. Vaithiligam, S. *et al.* *Ultrasonics Symposium*, 2007, 2611–2614 (2007).
21. Weissleder, R. & Ntziachristos, V. Shedding light onto live molecular targets. *Nature Med.* **9**, 123–128 (2003).
22. Razansky, D., Distel, M., Vinegoni, C., Ma, R. & Ntziachristos, V. Multispectral opto-acoustic tomography of deep-seated fluorescent proteins *in vivo*. *Opt. Express* **17**, 8769–8780 (2009).
23. Cai, W. *et al.* Peptide-labelled near-infrared quantum dots for imaging tumour vasculature in living subjects. *Nano Lett.* **6**, 669–676 (2006).
24. Schipper, M. L. *et al.* A pilot toxicology study of single-walled carbon nanotubes in a small sample of mice. *Nature Nanotech.* **3**, 216–221 (2008).
25. Kam, N. W., O'Connell, M., Wisdom, J. A. & Dai, H. Carbon nanotubes as multifunctional biological transporters and near-infrared agents for selective cancer cell destruction. *Proc. Natl Acad. Sci. USA* **102**, 11600–11605 (2005).
26. American National Standards Institute. *American national standard for the safe use of lasers.* ANSI Standard Z136.1–2000 (ANSI, New York, 2000).
27. Loening, A. M. & Gambhir, S. S. AMIDE: a free software tool for multimodality medical image analysis. *Mol. Imaging* **2**, 131–137 (2003).

Supplementary information accompanies this paper at www.nature.com/naturenanotechnology.

2. Paper submitted to Nature Photonics:

Ultra-High Sensitivity Carbon Nanotube Agents for Photoacoustic Molecular Imaging in Living Mice

Adam de la Zerda[1,2,*], Zhuang Liu[3,4,*], Sunil Bodapati[1], Robert Teed[1], Srikant Vaithilingam[2], Butrus T. Khuri-Yakub[2], Xiaoyuan Chen[1,5], Hongjie Dai[3,†], Sanjiv Sam Gambhir[1,6,†]

[1]Molecular Imaging Program at Stanford, Department of Radiology and Bio-X Program, the [2]Department of Electrical Engineering and the [3]Department of Chemistry, Stanford University, Palo Alto, CA 94305, USA.

[4]Functional Nano & Soft Materials Laboratory (FUNSOM), Soochow University, Suzhou, Jiangsu, 215123, China

[5]Laboratory for Molecular Imaging and Nanomedicine, National Institute of Biomedical Imaging and Bioengineering (NIBIB), National Institutes of Health (NIH), Bethesda, MD 20892, USA

[6]Department of Bioengineering, Stanford University, Palo Alto, CA 94305, USA.

* These authors contributed equally to this work

† e-mail: sgambhir@stanford.edu; hdai1@stanford.edu

Introduction

Photoacoustic imaging is an emerging modality that overcomes to a great extent the resolution and depth limitations of optical imaging while maintaining high-contrast[1-6]. However, since many diseases will not manifest an endogenous photoacoustic contrast, it is essential to develop exogenous photoacoustic contrast agents that can target diseased area(s). Recently, we showed that single-walled carbon nanotubes (SWNTs) have utility as targeted photoacoustic contrast agents[7]. Here we present a dye-enhanced SWNT agent that markedly increases the photoacoustic contrast in living tissues by 300-times compared to plain SWNTs, leading to sub-nanomolar sensitivities. By attaching two different dyes onto the SWNT surface, we show that the two resulting particles can be imaged simultaneously (multiplexing). Intravenous administration of targeted dye-enhanced SWNTs to tumor-bearing mice showed significantly higher signal in the tumor than mice injected with untargeted particles. Finally, we show that the new dye-enhanced SWNTs can detect ~20-times less cancer cells than previously reported SWNTs.

Results

We have recently reported on the conjugation of cyclic Arg-Gly-Asp (RGD) peptides to pegylated SWNTs[8] and their use as photoacoustic imaging agents[7]. In order to enhance the photoacoustic signal of the SWNTs, we attached Indocyanine Green (ICG) and QSY-21 dyes to the surface of the SWNTs through pi-pi stacking interactions[9] (see Methods section for more details). The ultra-high surface area of SWNTs allows highly efficient loading of aromatic molecules such as ICG and QSY-21 on the nanotube surface. This created two new kinds of photoacoustic agents; SWNT-ICG and SWNT-QSY (**Fig. 1a)**. The particles were targeted using the RGD-peptide to $\alpha_v\beta_3$ integrins, which are over-expressed in tumor vasculature, while control untargeted particles were synthesized using a non-targeted peptide, RAD.

The optical absorbance spectra of the two new particles suggest that 710 nm and 780 nm are the preferable wavelengths for scanning SWNT-QSY and SWNT-ICG respectively (**Fig. 1b**). At their respective absorbance peaks, the SWNT-QSY and SWNT-ICG particles exhibit a 17 and 20-fold higher absorbance respectively as compared with plain SWNTs. Since blood absorption is significantly reduced at 780 nm compared to 710 nm, SWNT-ICG was the particle of choice for the small animal experiments for this study. Importantly, the attachment of RGD or RAD peptides to SWNT-ICG had little effect on the particles' absorbance. We constructed a non-absorbing and non-scattering agarose phantom with inclusions of SWNT-ICG-RGD at increasing concentrations from 0.5 nM to 121.5 nM in multiples of 3 (n = 3 samples of each concentration). The photoacoustic signal produced by the SWNT-ICG-RGD particles correlated well with the nanoparticle concentration (R^2=0.983) (**Fig. 1c**).

We further validated that the new particles are stable in serum (**see Supplementary Information** and **Fig. S1**). The particle's photobleaching (loss of optical absorption due to continuous light exposure) was characterized and found to be relatively small, 30% bleaching over 60 min of typical laser irradiation (**see**

Supplementary Information and **Fig. S2**). Finally, cell uptake studies showed specific binding of SWNT-ICG-RGD to U87MG cells compared with the control particles SWNT-ICG-RAD (**see Supplementary Information** and **Fig. S3**).

We then tested the particle's sensitivity in living subjects by subcutaneously injecting the lower back of mice (n = 3) with 30 μl of SWNT-ICG-RAD mixed with matrigel at increasing concentrations of 820 pM to 200 nM in multiples of 3. Matrigel alone produced no significant photoacoustic signal (data not shown). Upon injection, the matrigel solidified, fixing the SWNT-ICG-RAD in place and three-dimensional (3D) ultrasound and photoacoustic images of the inclusions were acquired (**Fig. 2a**). While the ultrasound images visualized the mouse anatomy (e.g., skin and inclusion edges), the photoacoustic images revealed the SWNT-ICG-RAD contrast in the mouse. The photoacoustic signal from each inclusion was quantified using a three dimensional region of interest (ROI) drawn over the inclusion. We observed a linear correlation ($R^2 = 0.97$) between the SWNT-ICG-RAD concentration and the corresponding photoacoustic signal (**Fig. 2b**). Tissue background signal was calculated as the average photoacoustic signal in areas where no contrast agent was injected. Extrapolation of the signal-concentration graph reveals that 170 pM of SWNT-ICG-RAD gives the equivalent photoacoustic signal as the tissue background (i.e., signal to background ratio = 1). This value represents over 300-times improvement in sensitivity compared to plain SWNTs.

Finally, we tested the nanoparticles targeting ability in living mice. Mice bearing U87MG tumor xenografts (150 mm^3 in size) were injected through the tail vein (IV) with 200 μl of either targeted SWNT-ICG-RGD or untargeted SWNT-ICG-RAD particles (n = 4 mice per group) at a concentration of 1.2 μM. We acquired 3D photoacoustic and ultrasound images of the entire tumor area before and up to 4 hours after the injection. Mice injected with the targeted SWNT-ICG-RGD particles show significantly higher photoacoustic signal in the tumor compared with the control group (**Fig. 3a**). The ultrasound images were used for visualizing the boundaries of the tumor as well as to validate that no significant movement (beyond 100 μm) had occurred throughout the scan. While the pre-injection photoacoustic signal is primarily due to the tumor's blood content, post-injection photoacoustic signal consists of both blood and SWNT-ICG. To subtract out the blood signal from the images, a subtraction image calculated as the 2 hour post-injection minus the pre-injection image was calculated. Measurement of the photoacoustic signal from a 3D ROI around the tumor (**Fig. 3b)** showed that the photoacoustic signal in the tumor was significantly higher in mice injected with SWNT-ICG-RGD as compared with the control particles SWNT-ICG-RAD ($p < 0.001$). For example, at 2 hours post-injection, mice injected with SWNT-ICG-RGD showed over 100% higher photoacoustic signal in the tumor than mice injected with the control SWNT-ICG-RAD.

To compare the performance of plain SWNT-RGD to SWNT-ICG-RGD, we incubated U87MG cells, which express the target $\alpha_v\beta_3$ on their surface, with either particle solution for 2 hours. After incubation, the

cells were washed 3 times with cold saline to remove unbound particles and placed in a phantom at increasing concentrations from $25x10^3$ to $6x10^6$ cells per well (n = 3 samples per group) and imaged with the photoacoustic system (**Fig. 4a**). Quantitative analysis of the photoacoustic signal from the phantom revealed that cells exposed to SWNT-ICG-RGD were detected at 20-times lower concentration than cells exposed to plain SWNT-RGD ($p < 0.0001$) (**Fig. 4a-b**). These observations are consistent with the optical absorbance of SWNT-ICG-RGD being ~20 times higher than plain SWNT-RGD.

Finally, we show that the two kinds of photoacoustic imaging agents we synthesized, SWNT-ICG and SWNT-QSY can be imaged simultaneously due to their unique, though overlapping, absorbance spectra (**Fig. 1b**). We created an agarose gel phantom containing increasing concentrations of SWNT-ICG and decreasing concentrations of SWNT-QSY (starting from 100nM:0nM up to 0nM:100nM respectively). Photoacoustic images of the phantom were taken at wavelengths of 700, 730, 760, 780, and 800 nm and a spectral un-mixing algorithm was then used to separate each particle's signal to an individual image (**Fig. 5**).

We have synthesized, characterized and demonstrated the application of dye-enhanced SWNTs as ultra-high sensitivity photoacoustic imaging agents. A concentration of 170 pM was estimated to produce an equivalent photoacoustic signal as tissue background signal, representing 300-times higher sensitivity than plain SWNTs in living mice. This improvement is likely due to both the higher optical absorption of the particles as well as the fact that the new particle's absorption peak is at 780nm where the background tissue photoacoustic signal is greatly reduced. Intravenous injection of RGD-targeted SWNT-ICG particles to tumor-bearing mice led to significantly greater accumulation of the particles in the tumor compared to non-targeted control particles. We demonstrated the ability to multiplex 2 kinds of dye-enhanced SWNTs and showed the ability to detect 20-times fewer cancer cells when using SWNT-ICG-RGD as the imaging agent, as compared with plain SWNT-RGD. These results agree with the fact that SWNT-ICG has ~20 times greater optical absorbance compared to plain SWNT. Applications of the enhanced particles may therefore be exploited to lead to the earlier detection of cancer by providing the ability to detect smaller tumors.

The *in-vivo* targeting study results are likely negatively influenced by the effect of photo-bleaching, where continued laser light exposure of tumor causes reduction in the optical absorption (and photoacoustic signal) of particles that are bound to the tumor. This particularly affect the targeted group, SWNT-ICG-RGD, and to a much lesser extent the untargeted group, SWNT-ICG-RAD, which continue to circulate through the animal's blood stream unexposed to laser irradiation. Therefore, it is likely that the difference between these two groups is even greater in reality than reflected in the results.

Most of the work done on photoacoustic contrast agents has been focused on gold nanoparticles[10-12] as well as other kinds of nanoparticles[13, 14]. However, the main challenge that has yet been solved is the delivery of such agents to the tumor in sufficient amounts to create detectable and specific signal. This is likely due to the

particles' large size that leads to rapid clearance by the reticuloendothelial system (RES) upon intravenous injection, preventing the particles from accumulating at the tumor site. In contrast, the SWNTs used here are 1-2 nm in diameter and 50-300 nm in length. Since the dye we used was attached to the surface of the SWNTs, under the PEG, it is expected that the total particle size was not significantly changed, thereby allowing the particles to keep a favorable bio-distribution as previously reported[8]. Hence, the dye-enhanced SWNTs presented in this work offer unprecedented photoacoustic signal strengths while maintaining relatively small size allowing them to target tumors upon intravenous injection. We have also previously published pilot toxicology studies of the SWNTs with encouraging results in mouse models[15] as well as observed they are able to be excreted via the biliary pathway[16].

The reason for loading a SWNT with many small dye molecules is the high efficiency of optical absorption of these dyes as compared to their weight. By this measure of absorption divided by weight, ICG is 7-times more efficient than SWNT and ~8500-times more efficient than commercial gold nanorods with peak absorption at 780 nm.

The dye-enhanced SWNT photoacoustic contrast agents reported here have the capability to bind to molecular targets while maintaining a high photoacoustic signal. No other imaging modalities or reported imaging agents have the precise depth information and sub-millimeter spatial resolution at sub-nanomolar sensitivity that can be achieved with photoacoustic imaging of dye-enhanced SWNTs.

Methods

Dye-enhanced SWNTs synthesis

A complete description of the synthesis of SWNT-RGD and SWNT-RAD can be found elsewhere[8]. 250nM SWNT-RGD or SWNT-RAD was incubated with 2mM Indocyanine Green (ICG) molecules for overnight. ICG (Spectrum Laboratory Products, CA) (20 mM) was dissolved in DMSO first and then added to SWNT water solutions with a final DMSO concentration of 10% by volume. Unbound ICG molecules were removed from the solution by filtration through 100 kDa centrifuge filters (Millipore) and washed for 6-8 times. The SWNTs used in this work were 50-300 nm in length and 1-2 nm in diameter. The molar concentrations are based on an average molecular weight of 170 kDa per SWNT (150 nm in length and 1.2 nm in diameter). SWNT-QSY particles were synthesized the same way except replacing ICG with QSY-21.

Statistical methods. For the SWNT-ICG tumor targeting experiment, we used a mixed effects regression of signal on fixed factors of time, the square of the time, and group, and random factor of mouse to test the hypothesis that mice injected with SWNT-ICG-RGD showed an increased photoacoustic signal over time in the tumor compared with the control group injected with SWNT-ICG-RAD. There were significant effects of group

(Group 1 higher than Group 2, p=.001), and linear and quadratic effects of time (p<.001 and p=.019, respectively). There was no significant interaction between group and time effects (p=.915). For the cell uptake studies, we used the 1-tailed student's t-test to test whether the group in which U87MG cells were exposed to SWNT-ICG-RGD had statistically higher signal than the group of cells that was exposed to SWNT-ICG-RAD. For the experiment comparing SWNT-ICG-RGD to SWNT-RGD in-vitro, signal was compared between groups by a Wilcoxon test stratified by cell concentration. All statistics were done with Stata Release 9.2 (StataCorp LP, College Station, TX).

Mouse arrangement in the photoacoustic system. All animal experiments were performed in compliance with the Guidelines for the Care and Use of Research Animals established by the Stanford University Animal Studies Committee. A complete description of the photoacoustic system can be found in the Supplementary Information. Female nude mice were used for all the photoacoustic studies. The mice that were scanned in the photoacoustic system were fully anesthetized using isoflurane delivered through a nose-cone. Prior to the photoacoustic scan, the areas of interest were covered with agar gel to stabilize the area and minimize any breathing and other motion artifacts. A saran-wrap water bath was placed on top of the agar gel. An ultrasonic transducer, placed in the water bath, was therefore acoustically coupled to the mouse tissues. This setup allowed the ultrasonic transducer to move freely in 3D while not applying any physical pressure on the mouse.

SWNT-ICG tumor targeting in living mice. Two groups of female nude mice (n = 3 in each group) 6-8 weeks old were inoculated subcutaneously at their lower right back with 10^7 U87MG cells (American Type Culture Collection, ATCC) suspended in 50 μl of saline (PBS pH 7.4 1X, Invitrogen). The tumors were allowed to grow to a volume of ~100-150 mm^3. Before the injection, photoacoustic and ultrasound images of the mice were taken. Photoacoustic excitation light was 780 nm to match the absorption peak of SWNT-ICG. The mice were then injected with 200μl of 1.2μM or either targeted SWNT-ICG-RGD or control SWNT-ICG-RAD into the tail-vein (IV). During the injection the mice positioning was not changed. After the injection, photoacoustic and ultrasound images were acquired at: 0.5, 1, 2, 3, 4 hrs. post-injection. The scanning area varied between mice depending on the tumor orientation, but typically was ~10 mm x 10 mm, with a step size of 0.25 mm. At 4 hr post-injection, the mice were sacrificed. Using AMIDE software[17], a three dimensional ROI was drawn over the tumor volume (which was clearly illustrated in the ultrasound images). The mean photoacoustic signal in the tumor ROI was calculated for each photoacoustic image.

References

1. Wang, L. V. Multiscale photoacoustic microscopy and computed tomography. Nat Photon 3, 503-509 (2009).
2. Oh, J. T. et al. Three-dimensional imaging of skin melanoma in vivo by dual-wavelength photoacoustic microscopy. J Biomed Opt 11, 34032 (2006).
3. Zhang, H. F., Maslov, K., Stoica, G. & Wang, L. V. Imaging acute thermal burns by photoacoustic microscopy. J Biomed Opt 11, 054033 (2006).
4. Wang, X., Xie, X., Ku, G., Wang, L. V. & Stoica, G. Noninvasive imaging of hemoglobin concentration and oxygenation in the rat brain using high-resolution photoacoustic tomography. J Biomed Opt 11, 024015 (2006).
5. Zhang, H. F., Maslov, K., Stoica, G. & Wang, L. V. Functional photoacoustic microscopy for high-resolution and noninvasive in vivo imaging. Nat Biotechnol 24, 848-51 (2006).
6. Razansky, D. et al. Multispectral opto-acoustic tomography of deep-seated fluorescent proteins in vivo. Nat Photon 3, 412-417 (2009).
7. de la Zerda, A. et al. Carbon nanotubes as photoacoustic molecular imaging agents in living mice. Nat Nanotechnol 3, 557-62 (2008).
8. Liu, Z. et al. In vivo biodistribution and highly efficient tumour targeting of carbon nanotubes in mice. Nat Nano 2, 47-52 (2007).
9. Liu, Z., Sun, X., Nakayama-Ratchford, N. & Dai, H. Supramolecular Chemistry on Water-Soluble Carbon Nanotubes for Drug Loading and Delivery. ACS Nano. 1, 50-56 (2007).
10. Kim, J. W., Galanzha, E. I., Shashkov, E. V., Moon, H. M. & Zharov, V. P. Golden carbon nanotubes as multimodal photoacoustic and photothermal high-contrast molecular agents. Nat Nanotechnol 4, 688-94 (2009).
11. Eghtedari, M. et al. High sensitivity of in vivo detection of gold nanorods using a laser optoacoustic imaging system. Nano Letters 7, 1914-8 (2007).
12. Yang, X., Skrabalak, S. E., Li, Z. Y., Xia, Y. & Wang, L. V. Photoacoustic tomography of a rat cerebral cortex in vivo with au nanocages as an optical contrast agent. Nano Lett 7, 3798-802 (2007).
13. Kim, G. et al. Indocyanine-green-embedded PEBBLEs as a contrast agent for photoacoustic imaging. J Biomed Opt 12, 044020 (2007).
14. Zhang, Q. et al. Gold nanoparticles as a contrast agent for in vivo tumor imaging with photoacoustic tomography. Nanotechnology 20, 395102 (2009).
15. Schipper, M. L. et al. A pilot toxicology study of single-walled carbon nanotubes in a small sample of mice. Nat Nano 3, 216-221 (2008).
16. Liu, Z. et al. Circulation and long-term fate of functionalized, biocompatible single-walled carbon nanotubes in mice probed by Raman spectroscopy. Proc Natl Acad Sci U S A 105, 1410-5 (2008).
17. Loening, A. M. & Gambhir, S. S. AMIDE: a free software tool for multimodality medical image analysis. Mol. Imaging 2, 131-7 (2003).

Acknowledgments

We would like to acknowledge funding from the National Institute of Health (NIH) grants NCI CCNE U54 CA119367 (SSG), NCI ICMIC P50 CA114747 (SSG) for supporting this work. A. de la Zerda is partially funded from the Bio-X Graduate Student Fellowship and the DoD Breast Cancer Research Program – Pre-doctoral Traineeship Award. The authors would also like to thank J. Rosenberg for the statistical analysis and Omer Oralkan and Te-Jen Ma for useful discussions.

Figures:

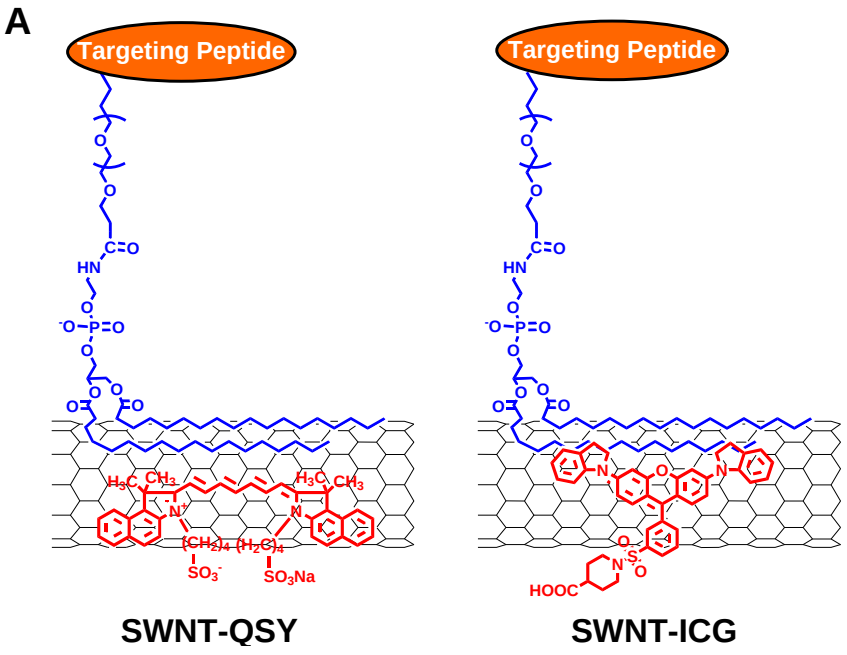
A
Targeting Peptide
Targeting Peptide
SWNT-QSY
SWNT-ICG

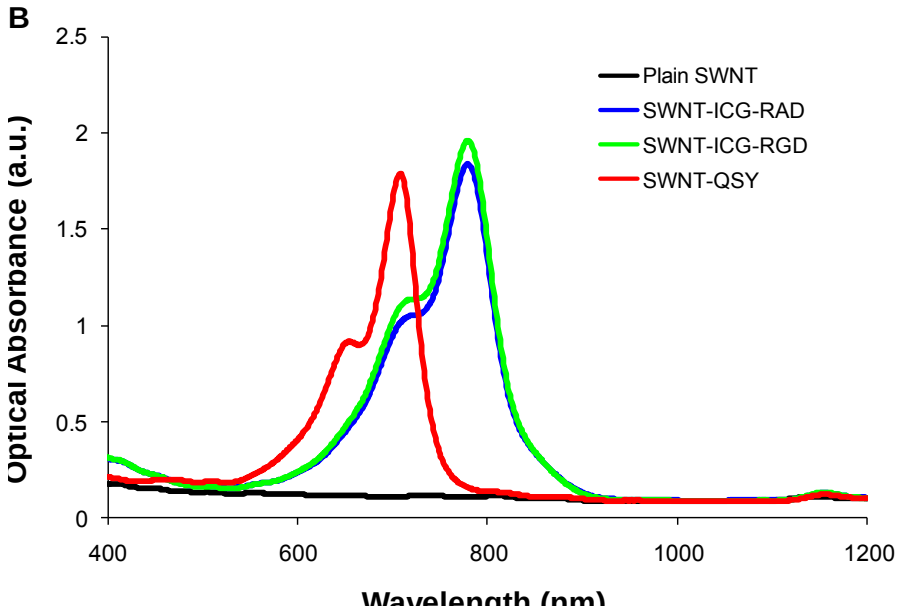
B
Optical Absorbance (a.u.)
2.5
2
1.5
1
0.5
0
400
600
800
1000
1200
Wavelength (nm)
Plain SWNT
SWNT-ICG-RAD
SWNT-ICG-RGD
SWNT-QSY

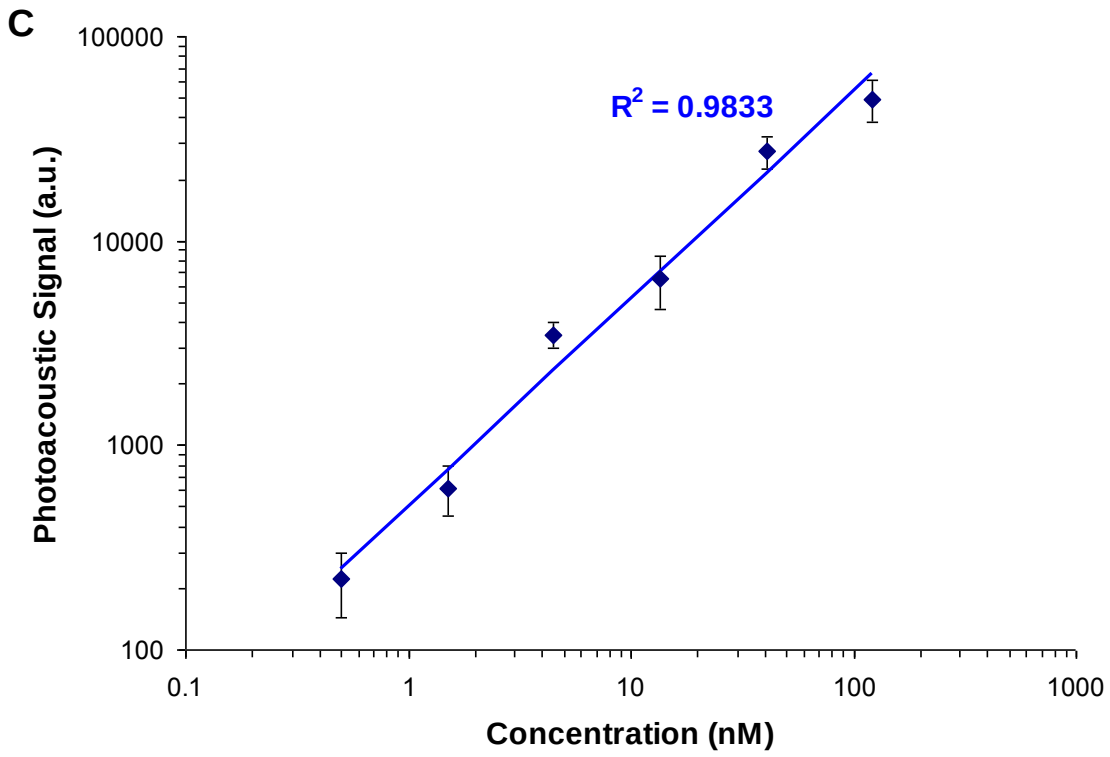

Figure 1. Characterization of the dye-enhanced SWNT. a, Illustration of SWNT-ICG and SWNT-QSY. ICG and QSY-21 (red molecules) are attached to the SWNT surface through non-covalent pi-pi stacking bonds. Polyethylene glycol-5000 (blue molecules) is conjugated to a targeting peptide in one end and to the SWNT surface on the other end through phospholipids. **b,** Optical spectra of plain SWNT (green), SWNT-ICG-RGD (red), SWNT-ICG-RAD (blue) and SWNT-QSY-RGD (black). The similarity of SWNT-ICG-RAD and SWNT-ICG-RGD spectra suggests that the peptide conjugation does not notably perturb the photoacoustic signal. **c,** The photoacoustic signal produced by SWNT-ICG was observed to be linearly dependent on the concentration ($R^2 = 0.9833$).

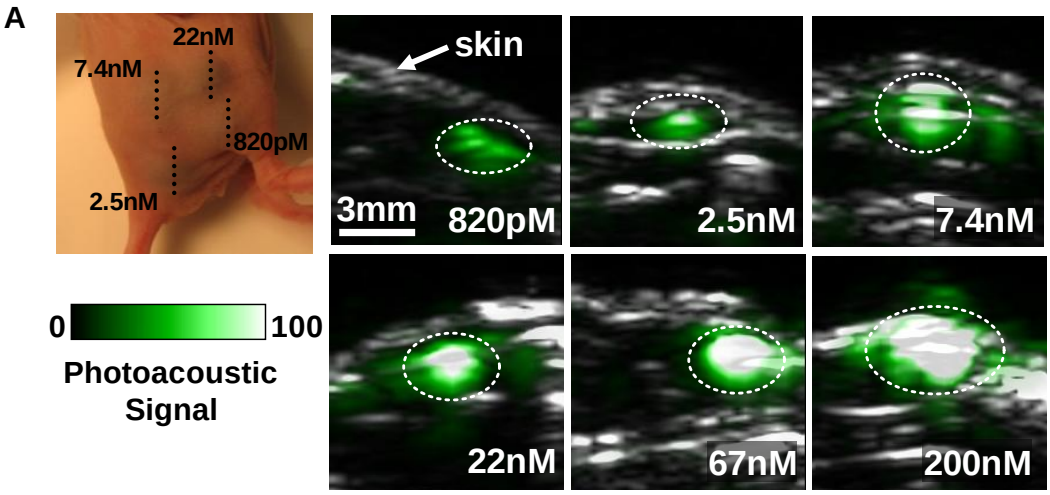

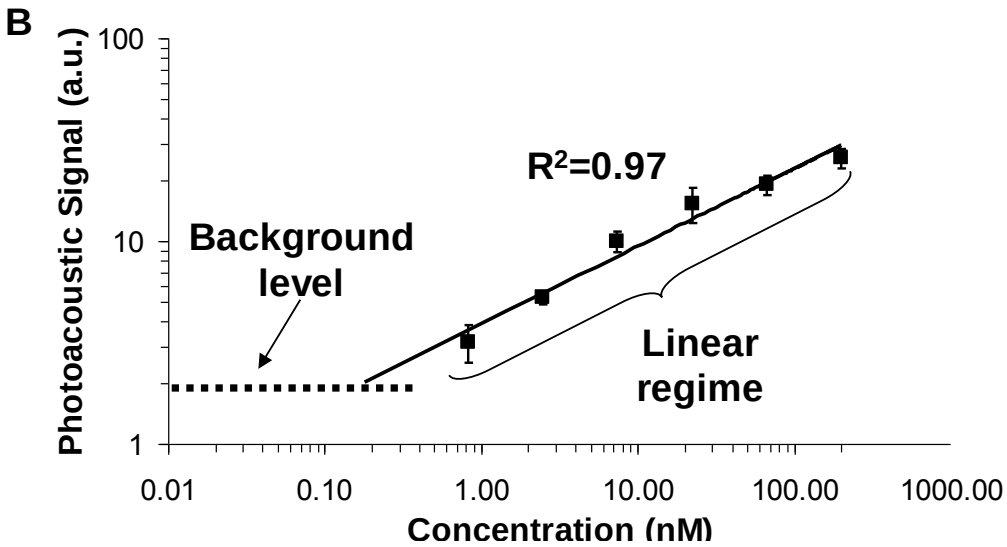

Figure 2. Photoacoustic detection of SWNT-ICG in living mice. a, Mice were injected subcutaneously with SWNT-ICG at concentrations of 0.82-200 nM. The images represent ultrasound (gray) and photoacoustic (green) vertical slices through the subcutaneous injections (dotted black line). The skin is visualized in the ultrasound images, while the photoacoustic images show the SWNT-ICG distribution. The white dotted lines on the images illustrate the approximate edges of each inclusion. **b,** The photoacoustic signal from each inclusion was calculated using 3D regions of interest and the 'background' represents the endogenous signal measured from tissues. The error bars represent standard error (n = 3 mice). Linear regression (R^2 = 0.97) of the photoacoustic signal curve estimates that a concentration of 170 pM of SWNT-ICG will give the equivalent background signal of tissues.

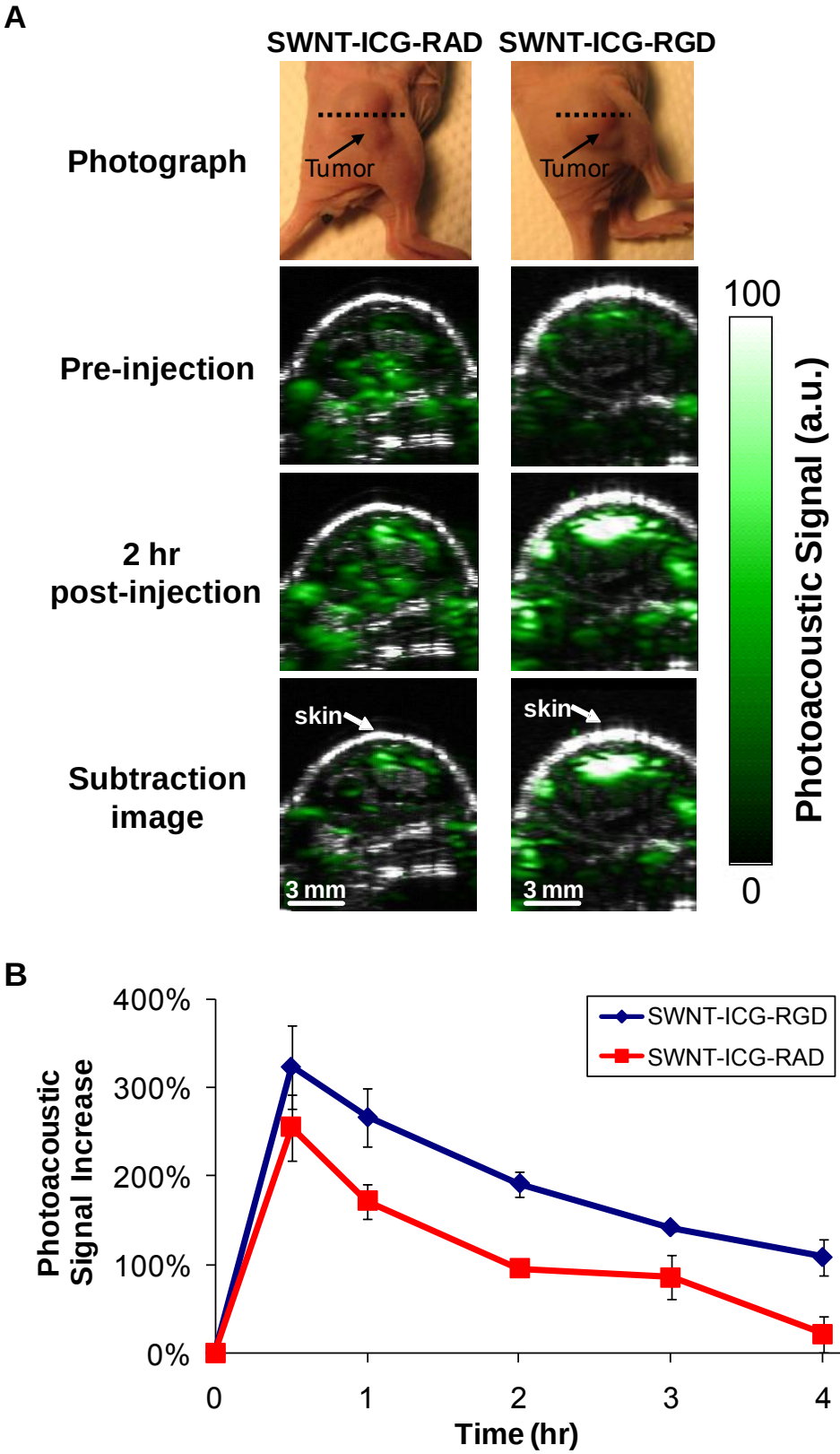

Figure 3. SWNT-ICG-RGD tumor targeting in living mice. a, Ultrasound (gray) and photoacoustic (green) images of one vertical slice through the tumor (dotted black line). The ultrasound images show the skin and the tumor boundaries. Subtraction photoacoustic images were calculated as 2 hr post-injection minus pre-injection images. As can be seen in the subtraction images, SWNT-ICG-RGD accumulates in higher amount in the tumor

as compared to the control SWNT-ICG-RAD. **b,** Mice injected with SWNT-ICG-RGD showed significantly higher photoacoustic signal than mice injected with the untargeted control SWNT-ICG-RAD ($p < 0.001$). The error bars represent standard error (n = 4 mice)

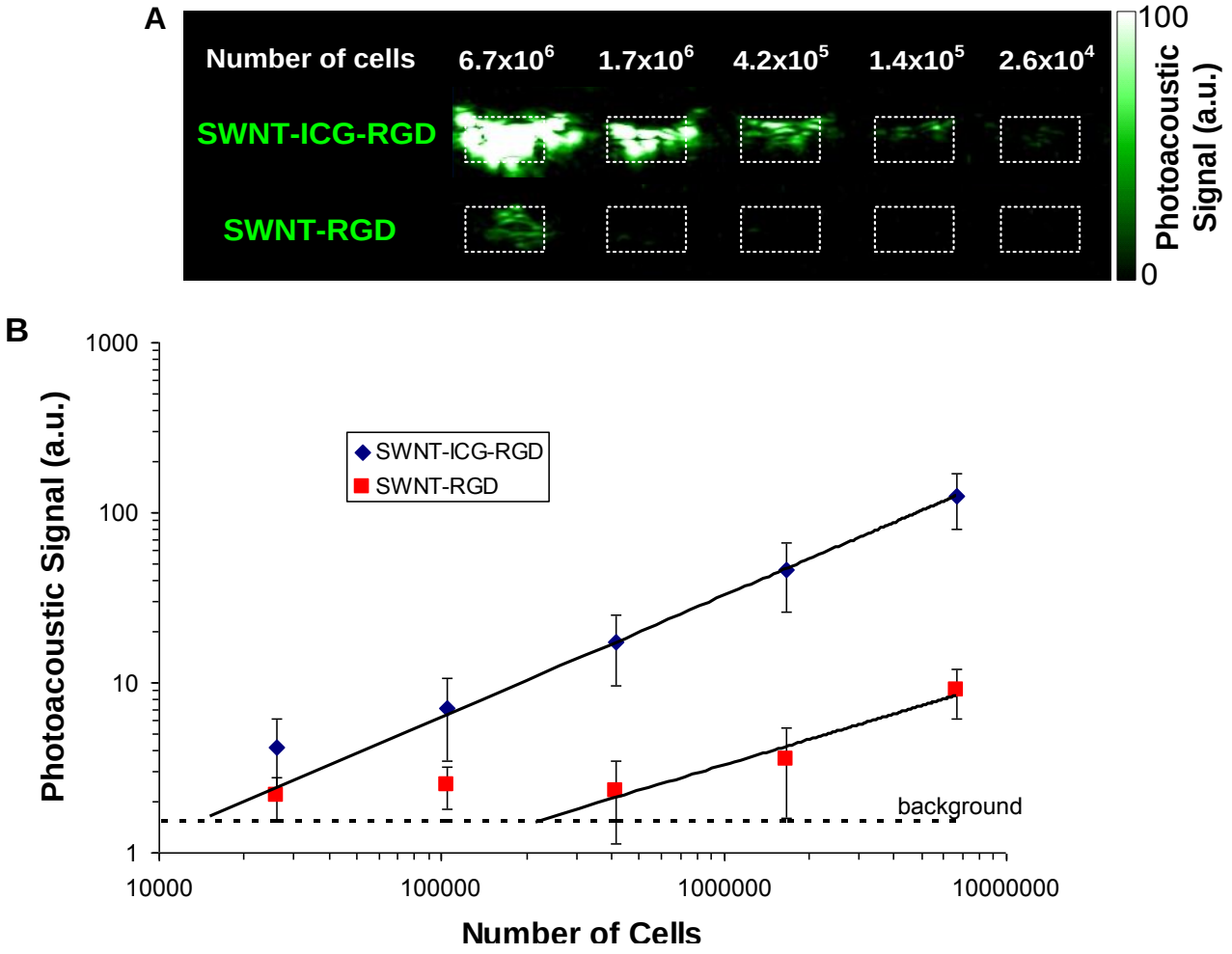

Figure 4. Comparison of plain SWNT-RGD to SWNT-ICG-RGD. a. Photoacoustic vertical slice image through a gel phantom containing increasing number of cells exposed to SWNT-ICG-RGD and SWNT-RGD. While $1.7x10^6$ cells exposed to SWNT-RGD are barely seen on the image, a clear photoacoustic signal was observed from $1.4x10^5$ cells exposed to SWNT-ICG-RGD. The signal inside the ROI (dotted white boxes) is not homogenous due to possible aggregates of cells. **b.** Quantitative analysis of the photoacoustic signals from the phantom (n = 3) showed that SWNT-ICG-RGD can see ~20-times less cancer cells than SWNT-RGD can ($p < 0.0001$). The background line represents the average background signal in the phantom. Linear regression was calculated on the linear regime of both curves.

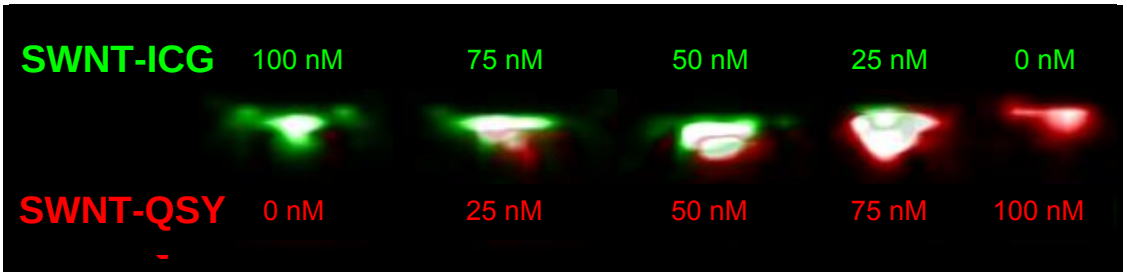

Figure 5. Multiplexing of SWNT-ICG with SWNT-QSY particles in a phantom. A phantom with various concentrations of SWNT-ICG and SWNT-QSY was scanned under the photoacoustic instrument at wavelengths of 700, 730, 760, 780, and 800 nm. A spectral un-mixing algorithm based on least-squares was used to separate the signals of SWNT-ICG particles (green) from SWNT-QSY particles (red). Notice that no SWNT-QSY signal is seen in the well with pure SWNT-ICG and vice versa, despite the fact that the two particles have overlapping spectra.

3. Abstract presented SPIE 2009:

Title: Photoacoustic Molecular Imaging using Single Walled Carbon Nanotubes in Living Mice

Authors: Adam de la Zerda[1,2], Cristina Zavaleta[1], Shay Keren[1], Srikant Vaithilingam[2], Sunil Bodapati[1], Robert Teed[1], Zhuang Liu[3], Jelena Levi[1], Bryan R. Smith[1], Te-Jen Ma[2], Omer Oralkan[2], Zhen Cheng[1], Xiaoyuan Chen[1], Hongjie Dai[3], Butrus T. Khuri-Yakub[2], Sanjiv S. Gambhir[1,4]

Abstract Text for Online or Printed Programs (100 words, early release)

Photoacoustic molecular imaging is an emerging modality offering non-invasive high resolution imaging of diseases using an external photoacoustic imaging agent. Here we demonstrate for the first time the utility of single walled carbon nanotubes as disease-targeted photoacoustic imaging agents in living mice. The carbon nanotubes were conjugated to RGD-peptides to target the $\alpha_v\beta_3$ integrin that is associated with tumor angiogenesis. Intravenous administration of these targeted carbon nanotubes to tumor-bearing mice showed significantly higher photoacoustic signal in the tumor as compared to non-targeted carbon nanotubes. These results were verified ex-vivo using a Raman microscope that is sensitive to SWNTs Raman signal.

Keywords:
Photoacoustic Imaging
Opotoacoustic Imaging
Molecular Imaging
Carbon Nanotubes

Abstract Text for Technical Review Purposes (250 words, publicized during the meeting)

Photoacoustic molecular imaging is an emerging technology offering non-invasive high resolution imaging of the molecular expressions of a disease using a photoacoustic imaging agent. Here we demonstrate for the first time the utility of single walled carbon nanotubes (SWNTs) as targeted imaging agents in living mice bearing tumor xenografts. SWNTs were conjugated with polyethylene-glycol-5000 connected to Arg-Gly-Asp (RGD) peptide to target the $\alpha_v\beta_3$ integrin that is associated with tumor angiogenesis.

In-vitro, we characterized the photoacoustic spectra of the particles, their signal linearity and tested their uptake by $\alpha_v\beta_3$-expressing cells (U87MG). The photoacoustic signal of SWNTs was found not to be affected by the RGD conjugation to the SWNTs and was also found to be highly linear with concentration ($R^2 = 0.9997$ for 25-400nM). The cell uptake studies showed that RGD-targeted SWNTs gave 75% higher photoacoustic signal than non-targeted SWNTs when incubated with U87MG cells.

In-vivo, we measured the minimal detectable concentration of SWNTs in living mice by subcutaneously injecting SWNTs at increasing concentrations. The lowest detectable concentration of SWNTs in living mice was found to be 50nM. Finally, we administered RGD-targeted and non-targeted SWNTs via the tail-vein to U87MG tumor-bearing mice (n=4 for each group) and measured the signal from the tumor before and up to 4 hours post-injection. At 4 hours post-injection, tumors of mice injected with RGD-targeted SWNTs showed 8 times higher photoacoustic signal compared with mice injected with non-targeted SWNTs. These results were verified ex-vivo using a Raman microscope that is sensitive to the SWNTs Raman signal.

4. Abstract 2 presented at SPIE 2009:

Enhanced Sensitivity Targeted Photoacoustic Molecular Imaging Agents in Living Mice

Adam de la Zerda, Zhuang Liu, Cristina Zavaleta, Sunil Bodapati, Robert Teed, Srikant Vaithilingam, Te-Jen Ma, Omer Oralkan, Xiaoyuan Chen, Butrus T. Khuri-Yakub, Hongjie Dai, Sanjiv Sam Gambhir

Abstract Text for Online or Printed Programs (100 words, early release)
Photoacoustic imaging of living subjects offers significantly higher spatial resolution at increased tissue depths compared to purely optical imaging techniques. We developed a new version of extremely bright photoacoustic imaging agent based on single walled carbon nanotubes (SWNTs) and the small molecular dye Indocyanine Green (ICG). We measured the photoacoustic signal from the new particle in-vitro and in-vivo and found it is 17-times higher than plain SWNTs. We conjugated the particles to RGD-peptides to target the $\alpha_v\beta_3$ integrin associated with tumor angiogenesis and showed that it can bind selectively to tumors when injection intravenously to living mice.

Abstract Text for Technical Review Purposes (250 words, publicized during the meeting)
Photoacoustic imaging of living subjects offers high spatial resolution at increased tissue depths compared to purely optical imaging techniques. We have recently shown that intravenously injected single walled carbon nanotubes (SWNTs) can be used as targeted photoacoustic imaging agents in living mice using RGD peptides to target $\alpha_v\beta_3$ integrins.

We have now developed a new targeted photoacoustic imaging agent based on SWNTs and Indocyanine Green (SWNT-ICG) with absorption peak at 780nm. The photoacoustic signal of the new imaging agent is enhanced by ~17 times as compared to plain SWNTs. To synthesize this particle, SWNTs were coupled to RGD peptides through polyethylene glycol-5000 grafted phospholipid. ICG molecules were then attached to the surface of each SWNT non-covalently through pi-pi stacking interactions.

In-vitro, we measured the serum stability of the particles and through cell uptake studies with U87MG cells, we verified that the particles bind selectively to $\alpha_v\beta_3$ integrin. In-vivo, we injected the imaging agents subcutaneously to living mice (n=4) and were able to detect concentrations as low as 3nM, a 17-fold enhancement in sensitivity over plain SWNTs ($p<0.05$). Finally, we injected U87MG tumor-bearing mice (n=4) with RGD-targeted SWNT-ICG via the tail-vein. Control mice were injected with non-targeted SWNT-ICG. Upon administration, the RGD-targeted particles created a significantly higher photoacoustic signal in the tumors than the non-targeted particles ($p<0.05$). These results were verified ex-vivo using a Raman microscope sensitive to the SWNTs Raman signal.

In summary, the new SWNT-based particle can target tumors in living mice while possessing a very high photoacoustic signal.

5. Abstract presented at World Molecular Imaging Congress 2009

Ultra High Sensitivity Targeted Photoacoustic Imaging Agents for Cancer Early Detection in Living Mice

Adam de la Zerda[*], Zhuang Liu[*], Sunil Bodapati, Robert Teed, Cristina Zavaleta, Srikant Vaithilingam, Xiaoyuan Chen, Butrus T. Khuri-Yakub, Hongjie Dai[†], Sanjiv Sam Gambhir[†]

Photoacoustic molecular imaging of living subjects offers high spatial resolution at increased tissue depths compared to optical imaging strategies. We have recently demonstrated single walled carbon nanotubes (SWNTs) conjugated to Indocyanine Green (SWNT-ICG) as targeted photoacoustic imaging agents *in-vitro*.

In the current work, we created a significantly improved SWNT-ICG particle with over 1000-times better sensitivity than plain SWNT and demonstrated their ability to target tumors when injected intravenously to a living mouse.

The targeted SWNT-ICG particles were synthesized by coupling of ICG molecules to the surface of SWNT-RGD particles through pi-pi stacking interactions. Control SWNT-ICG particles were created using the untargeted SWNT-RAD instead.

We verified the particles are stable in serum and target $\alpha_v\beta_3$ integrin through cell uptake studies with U87 cells. We found the photoacoustic signal produced by the particles to be highly linear to their concentration both in phantom studies ($R^2 = 0.99$) as well as in living mice injected with the particles subcutaneously ($R^2 = 0.971$). We further measured the detection sensitivity of SWNT-ICG in living mice (n = 3 mice) and found it to be 30 pM. This represents more than 3 orders of magnitude improvement compared to plain SWNTs sensitivity in living mice ($p < 0.05$). Furthermore, xenograft-bearing mice were tail-vein injected with RGD-targeted SWNT-ICG. At 2 hours post-injection, mice injected with the RGD-targeted particles showed 2.1-times higher photoacoustic signal in the tumor compared to mice injected with control particles ($p < 0.05$, n = 4 mice). Finally, we demonstrated the superiority of the SWNT-ICG-RGD particles by incubating them with U87 cells and detecting in living mice 1000-times such cells than if the cells were incubated with plain SWNT-RGD.

This is the first photoacoustic imaging agent tested and targeted in living animals that we know of that can reach such a high sensitivity of 30 pM.

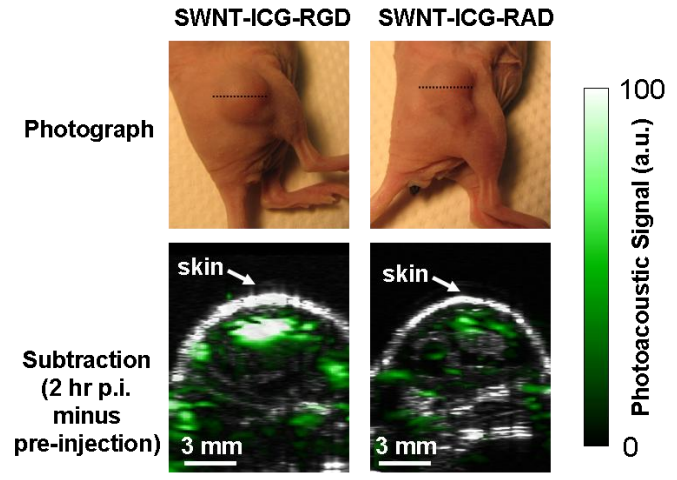

Mice injected with RGD-targeted SWNT-ICG showed significantly higher photoacoustic signal at 2 hours post-injection compared to mice injected with control particles